Article

Gut microbiota and brain-resident CD4⁺ T cells shape behavioral outcomes in autism spectrum disorder

John Chulhoon Park [1], Min-A Sim[1], Changhon Lee[1,4], Hye-Eun Park[1], Juhun Lee[2], Seung Yeon Choi [2], Seohyun Byun[1,5], Haeun Ko [1], Haena Lee [1], Seung Won Kim [1], Jaegyun Noh [1], Geon Park[1], Solji Lee [2], Tae-Kyung Kim [1,3] ✉ & Sin-Hyeog Im [1,2,3] ✉

Autism spectrum disorder (ASD) is a neurodevelopmental disorder characterized by alterations in social, repetitive, and anxiety-like behaviors. While emerging evidence suggest a gut-brain etiology in ASD, the underlying mechanisms remain unclear. To dissect this axis, we developed a germ-free BTBR mouse model for ASD. The absence of gut microbiota in male mice ameliorates ASD-associated behaviors and reduces populations of inflammatory brain-resident T cells. Additionally, CD4⁺ T cell depletion mitigates neuroinflammation and ASD behaviors, suggesting a gut-immune-brain axis. We identify several microbial and metabolic regulators of ASD, particularly those relevant to the glutamate/GABA ratio and 3-hydroxyglutaric acid. Using an in silico metabolite prediction model, we propose *Limosilactobacillus reuteri* IMB015 (IMB015) to be a probiotic candidate. Administration of IMB015 reduces the glutamate/GABA ratio and neuroinflammation, resulting in improved behaviors. Here we report a gut-immune-brain axis in which the gut microbiota and its metabolites can modulate brain-resident immune cells and ASD-associated behaviors.

Autism spectrum disorder (ASD) is a neurodevelopmental disorder with core behavioral features including social communication deficits and repetitive behaviors, with common comorbidities in neuropsychiatric symptoms such as anxiety and hyperactivity[1]. Complex interactions between intrinsic and extrinsic factors regulate ASD, such as host genetics and the gut microbiota. Recent milestone studies have demonstrated causal relations between the gut microbiota and ASD, suggesting a gut-brain mechanism. For instance, gut microbiota transfer from ASD patients into germ-free (GF) mice induces ASD-associated behaviors, attributing the gut microbiota and its metabolites as a major contributor to the disorder[2]. Further suggesting a gut-brain link, ASD patients harbor unique microbiome

signatures compared to neurotypical individuals. Numerous studies have identified several trends, with increased abundances of *Clostridium, Lactobacillus*, and *Faecalibacterium* and decreases in *Bifidobacterium, Enterococcus*, and *Streptococcus* in ASD[3]. The gut-brain axis in ASD has spurred interests in developing live biotherapeutic products (LBP) for the disorder. Several probiotic strains have demonstrated efficacy in preclinical studies, including *Lactobacillus reuteri* ATCC PTA 6475, *L. reuteri* RC-14, and *Bacteroides fragilis* NCTC 9343[4-7]. Although the efficacy of probiotics in human ASD patients remains uncertain, emerging research using *L. reuteri* ATCC PTA 6475 and DSM 179338 promises potential[8]. Importantly, the global prevalence of ASD continues to rise annually, and the combination of

[1]Department of Life Sciences, Pohang University of Science and Technology, Pohang, Republic of Korea. [2]ImmunoBiome Inc, Pohang, Republic of Korea. [3]Institute for Convergence Research and Education in Advanced Technology, Yonsei University, Seoul, Republic of Korea. [4]Present address: Department of Immunology, Blavatnik Institute, Harvard Medical School, Boston, MA, USA. [5]Present address: Celltrion, Inc., Incheon, Republic of Korea. ✉e-mail: tkkim@postech.ac.kr; iimsh@postech.ac.kr

limited treatments and the socioeconomic burdens of ASD underscores the need for urgent research.

The host immunity may serve as a link in the gut-brain axis. Many studies have correlated gastrointestinal disorders and immune dysfunction with ASD, suggesting a gut-immune-brain axis in the disorder[9]. The gut microbiota plays a fundamental role in regulating immune homeostasis and is closely associated with diverse disorders. Usage of GF mice has significantly expanded our understanding of how host-microbe interactions influence immune development[10]. GF mice show severe impairment in both mucosal and systemic T cell development, with loss of both pro-inflammatory and anti-inflammatory populations and functions, highlighting the necessity of gut microbes for normal immune development[11]. Along with its role on immune maturation, the gut microbiota may be essential for healthy brain development, as GF C57BL/6 (B6) mice have been characterized with disruptions in anxiety-like behaviors, hyperactivity, and memory functions compared to their specific pathogen-free (SPF) counterparts[12].

Although the brain has traditionally been regarded as an immune-privileged site, the discovery and characterization of unique brain-resident T cells in human and murine brains are reshaping this paradigm[13]. Much like in the periphery, different subsets of T cells within the brain drive or restrain disease. For instance, regulatory T cells (Tregs) in the brain can suppress inflammatory responses from microglia and macrophages, as well as mitigate neurotoxic astrogliosis[14,15]. Meanwhile, inflammatory cytokines such as IL-17a can potentiate neurological disorders in mice, including ASD and anxiety-like behaviors[16,17]. These few, yet substantial, insights into the niche capacity of brain-resident T cells underscore how little is known about their populations, functions, and potential to be therapeutic targets for neurological disorders.

In this study, we aim to elucidate the intricate mechanisms contributing to ASD by investigating the interactions among genetic predisposition, gut microbiota and their metabolites, and host immune responses. We utilize the BTBR T+ Itpr3tf/J (BTBR) mouse model for ASD, which is well-characterized with several genetic aberrations, including four single nucleotide polymorphisms in ASD candidate genes, that lead to ASD-associated behavioral phenotypes[18,19]. Additionally, BTBR mice have previously been characterized with systemic inflammation and gut microbial dysbiosis, suggesting a basis for a gut-immune-brain axis[20,21]. To investigate how the gut microbiota influences ASD symptoms, we have generated GF BTBR mice. In male GF BTBR mice, the absence of gut microbiota offsets multiple ASD-associated behaviors, alters neuronal activation, and shifts immune phenotypes within the brain. Given the gut microbiota's close regulation of host immunity, we assess whether a specific subset of immune cells mediates this effect. Depletion of CD4+ T cells alters microglial activity and successfully normalizes ASD-associated behaviors. Through gut microbiota and metabolite analyses, we identify a bacterium capable of driving ASD by promoting neuroinflammation and elevating ASD-associated metabolites. Using an in silico metabolite prediction model, we hypothesize that a probiotic candidate may demonstrate therapeutic efficacy. Administration of the probiotic strain mitigates ASD-associated behaviors by decreasing neuroinflammation and levels of ASD-related metabolites. These findings reveal critical axes modulating ASD in a genetic mouse model and propose an intervention pathway with potential therapeutic benefits.

Results

Gut microbiota influences the onset of ASD behavioral phenotypes by modulating neuronal activation

At 8 weeks of age, BTBR mice displayed reduced social preference compared to B6 mice during the three-chamber sociability test, as indicated by comparable or less time spent in the chamber with a target mouse (social chamber) as opposed to the chamber with an empty pencil cup (empty chamber) (Supplementary Fig. 1A). Social memory was assessed using the three-chamber social novelty test by measuring the time spent in the chamber with an unfamiliar mouse (novel chamber) compared to the chamber with a familiar mouse (familiar chamber). BTBR mice showed reduced social memory, as they had no preference between familiar and novel subjects, whereas B6 mice showed a strong interest in novel mice (Supplementary Fig. 1B). Repetitive behavior was assessed by using the marble burying test, during which the number of marbles buried reflect the level of compulsive-like and repetitive behavior[22]. BTBR mice buried a significantly higher percentage of marbles compared to B6 mice, marking a high degree of repetitive behavior (Supplementary Fig. 1C). Furthermore, BTBR mice showed impaired anxiety-like behaviors with greater time and frequency to the center zone during the open field maze, as previously reported (Supplementary Fig. 1D)[23]. Hyperlocomotion during the open field maze was also significantly elevated in BTBR mice compared to B6 mice (Supplementary Fig. 1E). BTBR mice have previously been characterized to show a high degree of self-grooming[24]. During the open field maze and the three-chamber assay, BTBR mice spent greater time self-grooming than B6 mice (Supplementary Fig. 1F, G). While frequent self-grooming is considered an ASD-associated behavior in mice, it may raise potential concerns as the excessive immobile durations may impede on participation in the behavior tests. However, BTBR mice exhibited increased locomotion during these behavior assays compared to B6 mice, suggesting that despite more self-grooming, their participation in the tests was not hindered (Supplementary Fig. 1E, H). The amygdala and the hippocampus are brain regions commonly associated with anxiety, hyperactivity, and social cognition. The behavioral abnormalities in BTBR mice coincided with greater neuronal activation in these brain regions, as measured by the number of c-FOS+ neurons (Supplementary Fig. 1I–K). Our initial results confirmed previous reports and characterized several ASD phenotypes in the BTBR mice.

Numerous studies have identified correlations between the gut microbiota and ASD. To precisely examine the role of the gut microbiota, we generated a line of germ-free BTBR mice (GF BTBR) through embryonic transfer and rearing in GF isolators. The absence of a gut microbiota in these mice did not affect sociability, as both GF and SPF BTBR mice showed no preference for the social chambers during the three-chamber sociability test (Fig. 1A). However, GF BTBR mice showed a clear preference for the novel chamber during the social novelty test, indicating neurotypical social memory (Fig. 1B). Additionally, GF BTBR mice displayed reduced repetitive behavior during the marble burying test (Fig. 1C). These GF mice also spent less time in the center zone during the open field maze compared to their SPF counterparts, signifying a normalization of anxiety-like behavior, similar to that of neurotypical B6 mice (Fig. 1D and Supplementary Fig. 1D). GF status did not affect locomotion during the open field maze (Fig. 1E). Alterations in ASD-associated behaviors indicate that the gut microbiota may regulate neuronal function. Immunofluorescence staining identified reduced c-FOS+ neurons in the amygdala and dentate gyrus in GF BTBR mice compared to SPF mice (Fig. 1F–H). These results suggest that despite genetic predisposition to ASD, the absence of a gut microbiota can prevent certain ASD behavioral phenotypes by altering neuronal activity within the brain.

The gut microbiota shapes brain-resident T cells and their inflammatory cytokine production

Inflammation is often correlated with ASD and is considered as a diagnostic biomarker for the disorder[25]. Mouse models of ASD, including BTBR mice, have been previously recorded to show peripheral immune dysregulation[21]. In concordance with these results, BTBR mice showed a higher frequency of CD4+ T cells and greater numbers of CD4+ and CD8+ T cells in the spleen than B6 mice (Supplementary Fig. 2A, B). These splenic CD4+ T cells in BTBR mice showed
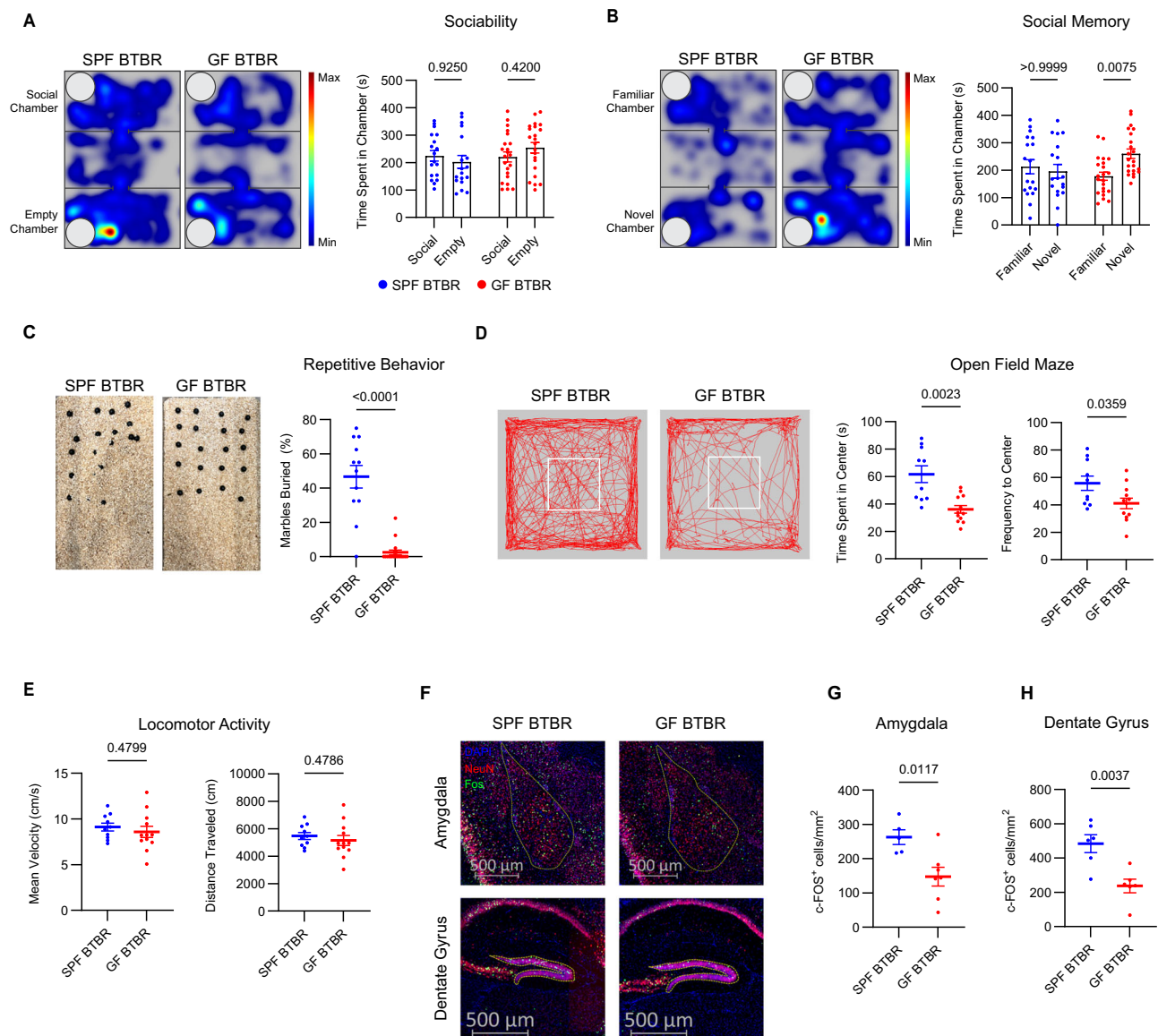
Fig. 1 | GF BTBR do not manifest ASD-associated phenotypes. A Representative heat maps and time spent in either the social or empty chambers during the three-chamber sociability test. SPF BTBR $n = 18$, GF BTBR $n = 22$. P value from two-way ANOVA, $F_{1,76} = 1.948$. **B** Representative heat maps and time spent in either the familiar or novel chambers during the three-chamber social novelty test. SPF BTBR $n = 18$, GF BTBR $n = 22$. P value from two-way ANOVA, $F_{1,76} = 5.817$. **C** Representative images and percent of marbles buried during the marble burying test. SPF BTBR $n = 12$, GF BTBR $n = 18$. $P = 0.000002$ from two-tailed Welch's t-test, $t(11.97) = 6.540$. **D** Representative traces, time spent in the center zone, and frequency to the center zone during the open field maze. SPF BTBR $n = 10$, GF BTBR $n = 12$. P value from two-tailed Welch's t-test, $t(12.76) = 3.785$ and $t(18.95) = 0.7207$, respectively. **E** Mean velocity and distance traveled during the open field maze. SPF BTBR $n = 10$, GF BTBR $n = 12$. P value from two-tailed Welch's t-test, $t(18.95) = 0.7207$ and $t(18.94) = 0.7229$. **F–H** Representative immunofluorescence staining and number of c-FOS+ neurons per area in the amygdala (two-tailed Student's t-test, $t(5) = 3.562$. SPF BTBR $n = 5$ sections, 3 mice, GF BTBR $n = 7$ sections, 4 mice) (**G**) and dentate gyrus of the hippocampus ($t(10) = 3.769$. SPF BTBR $n = 6$ sections, 3 mice, GF BTBR $n = 6$ sections, 3 mice) (**H**). All data represented as mean ± SEM. Source data are provided as source data file.

increased levels of IFN-γ, while CD8+ T cells showed a strong tendency (Supplementary Fig. 2C, D). In the colonic lamina propria, CD4+ and CD8+ T cells were also more enriched in BTBR mice, with reduced Foxp3+ regulatory T cell (Treg) populations (Supplementary Fig. 2E–G). Following, colonic Treg IL-10 production was reduced in BTBR mice (Supplementary Fig. 2H). Our analysis confirms immune dysregulation in BTBR mice, characterized with inflammatory T cells in the spleen and low Treg function in the gut.

Previous studies indicate that the gut microbiota is a critical regulator of host immunity, with microbial signals playing a central role in the proper development and function of the adaptive immune system[26]. Having observed inflammatory T cells in BTBR mice, we then questioned whether the inflammatory response and ASD-associated behaviors were connected by a microbiota-dependent mechanism. In the spleen, while the absence of microbiota slightly elevated the frequency of CD4+ T cells, there were no differences in the total cell numbers of CD4+ or CD8 T+ cells (Supplementary Fig. 3A, B). However, GF BTBR mice showed reduced IFN-γ levels in splenic CD4+ and CD8+ T cells (Supplementary Fig. 3C, D). In the colonic lamina propria, GF BTBR mice showed a reduced CD4+ T cell population without significant change in CD8+ cells (Supplementary Fig. 3E, F). Furthermore, both Treg and Foxp3- effector T cells (Teff) populations were reduced, followed by decreases in IL-10 and IFN-γ production in GF BTBR mice (Supplementary Fig. 3G–K). The immunological differences observed between SPF and GF BTBR mice parallel those seen in SPF and GF B6 mice, indicating that the influence of gut microbiota on host immunity
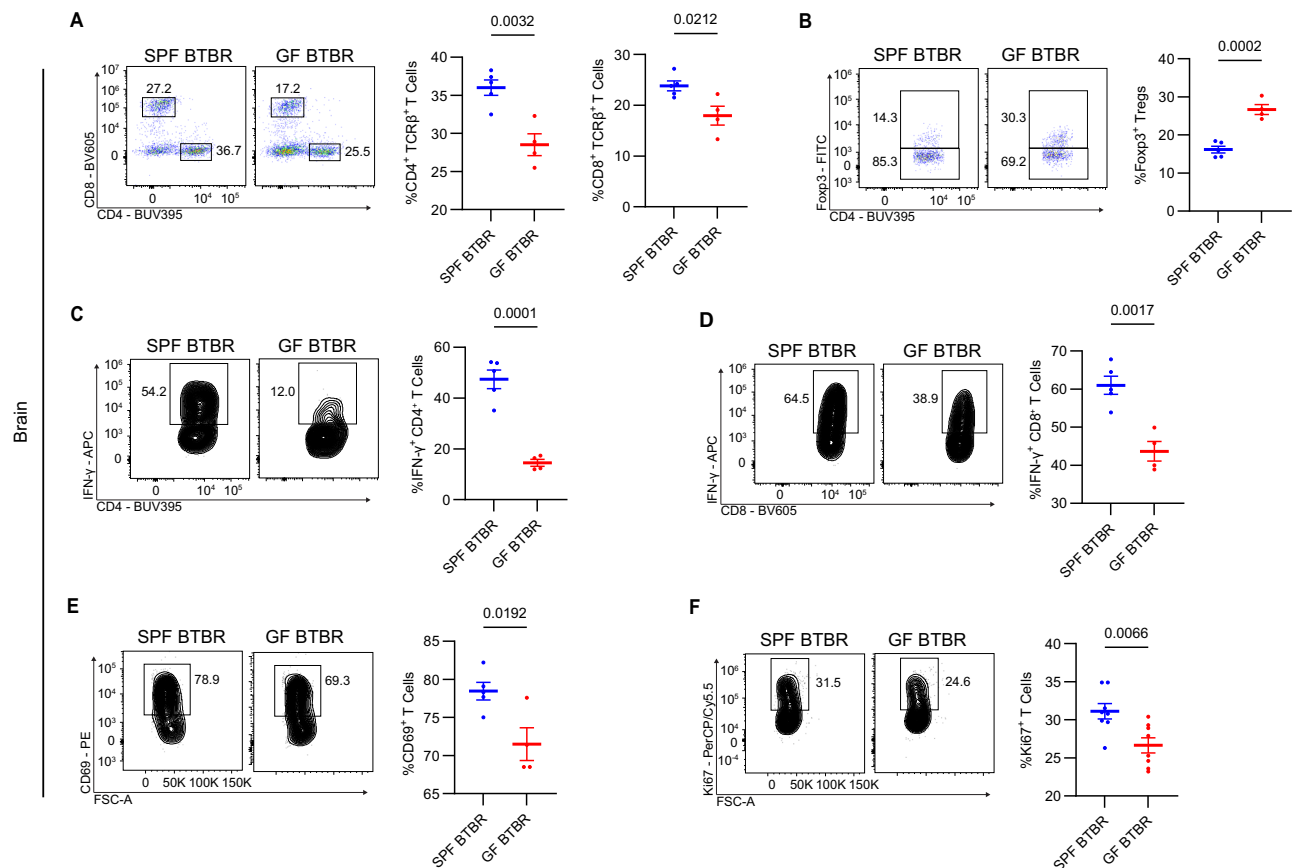
Fig. 2 | Microbiota regulates brain-resident T cells in BTBR mice.
A Representative flow cytometry plots and frequency of CD4+ or CD8+ T cells gated from TCRβ+ CD45+ live cells within the whole brain parenchyma of SPF or GF BTBR mice. SPF BTBR $n = 5$ mice, GF BTBR $n = 4$ mice. P values from two-tailed Student's t-test, $t(7) = 4.385$ and $t(7) = 2.958$, respectively. **B** Representative flow cytometry plots and frequency of Foxp3+ Tregs gated from CD4+ T cells in the brain. SPF BTBR $n = 5$ mice, GF BTBR $n = 4$ mice. P value from two-tailed Student's t-test, $t(7) = 6.887$.
C, D Representative flow cytometry plots and frequency of IFN-γ+ Foxp3- CD4+ T cells or IFN-γ+ CD8+ T cells in the brain parenchyma. SPF BTBR $n = 5$ mice, GF BTBR

$n = 4$ mice. P values from two-tailed Student's t-test, $t(7) = 7.625$ and $t(7) = 4.912$, respectively. **E** Representative flow cytometry plots and frequency of CD69+ T cells in the brain gated from TCRβ+ CD45+ cells. SPF BTBR $n = 5$ mice, GF BTBR $n = 4$ mice. P values from two-tailed Student's t-test, $t(7) = 3.028$. **F** Representative flow cytometry plots and frequency of Ki67+ T cells in the brain gated from CD45+ cells. SPF and GF BTBR $n = 8$ mice, P value from two-tailed Student's t-test, $t(14) = 3.185$. Flow cytometric analyses are representative results from at least 2 independent experiments with minimum of 4 mice. All data represented as mean ± SEM. Source data are available in source data file.

is conserved across murine strains[26]. Thus, our immune phenotyping demonstrates that the gut microbiota is required for intestinal and peripheral adaptive immune maturation in BTBR mice.

Given the recent discovery and characterization of brain-resident T cells, we sought to investigate their role in ASD and explore whether the brain-specific immune compartment serves as a bridge between peripheral and neuro-inflammation[27]. Whole brains were removed without the meninges, and immune cells were isolated by Percoll gradient for flow cytometry. Brain-resident T cells were gated from TCRβ+ cells within CD45high populations of live cells. Within the brain parenchyma, BTBR mice showed similar trends as in the periphery, with higher populations of brain-resident CD4+ and CD8+ T cells than B6 mice (Supplementary Fig. 4A, B). Furthermore, these brain-resident CD4+ and CD8+ T cells had higher levels of IFN-γ in BTBR mice, suggesting enhanced T cell-driven neuroinflammation (Supplementary Fig. 4C, D).

Next, we examined whether the gut microbiota affects brain-resident T cell populations in BTBR mice. Surprisingly, GF BTBR mice had reduced percentages of brain-resident CD4+ and CD8+ T cells compared to SPF BTBR mice, although there were no significant changes in the absolute cell numbers (Fig. 2A, Supplementary Fig. 4E). The absence of a gut microbiota also elevated the frequency of Tregs in the brain (Fig. 2B). Correspondingly, we observed reduced IFN-γ levels from CD4+ and CD8+ T cells in GF BTBR brains (Fig. 2C, D). Brain-

resident T cells have been characterized to express CD69, a marker of T cell activation as well as tissue-resident memory phenotype, which highlight their functional niche in the brain[13,28]. Along with reduced IFN-γ levels, T cells within the brains of GF BTBR mice had reduced CD69 and Ki67, suggesting that the gut microbiota may dictate both the functional activity and residency phenotype of brain-resident T cells (Fig. 2E, F). Our findings reveal that the gut microbiota modulates brain-resident T cells. Thus, the behavioral changes observed in GF BTBR mice may stem from the attenuation of T cell-mediated neuroinflammation.

CD4+ T cells regulate inflammatory microglia and ASD-associated behaviors

We aimed to explore the role of adaptive immunity as a regulator of ASD. CD4+ T cells, but not CD8+ T cells, have been identified as essential for the proper maturation of microglia, as well as hippocampal neurogenesis[13,27,29,30]. Additionally, CD4+, but not CD8+, T cells have been shown to regulate repetitive and anxiety-like behaviors in the B6 murine background[27,30,31]. To verify the role of CD4+ T cells in ASD etiology, CD4+ T cells were depleted in SPF BTBR mice through the administration of anti-CD4 monoclonal depletion antibody at postnatal day 5 (P5), P13, and P36 (Fig. 3A), as previously described[27]. At 8 weeks of age, CD4+ T cell depletion was confirmed in the spleen, draining lymph nodes, (Supplementary Fig. 5A–D) and
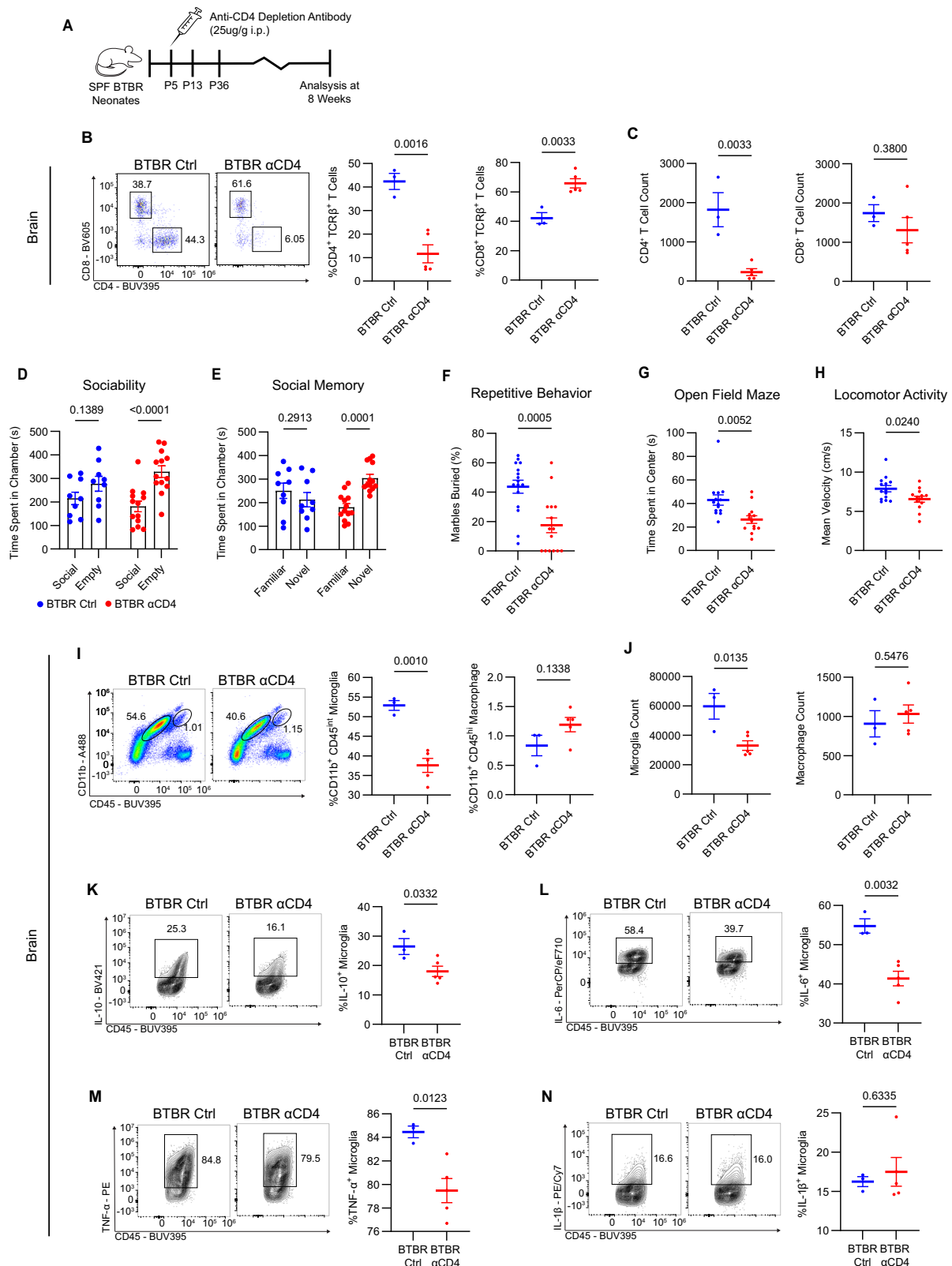
brain parenchyma, with no changes in CD8$^+$ T cell counts (Fig. 3B, C). CD4$^+$ T cell depletion improved social memory, but not sociability, as measured during the three-chamber tests (Fig. 3D, E). CD4$^+$ T cell depletion also led to a significant reduction in repetitive behavior (Fig. 3F). Furthermore, CD4$^+$ T cell-depleted BTBR mice spent reduced time and frequency in the center zone and showed reduced locomotor activity in the open field maze (Fig. 3G, H and Supplementary Fig. 5E,

F). These findings mirror many of the phenotypes observed in GF BTBR and healthy B6 mice, underscoring a link between the gut microbiota and CD4$^+$ T cells in ASD pathology.

Given the role of CD4$^+$ T cells in microglia maturation, we examined whether depleting CD4$^+$ T cells in BTBR mice affected other immune populations in the brain. The absence of CD4$^+$ T cells resulted in reduced microglia populations without significant changes in the

Fig. 3 | Depletion of CD4⁺ T cells abrogate ASD-associated behaviors and neuroinflammation. A SPF BTBR pups were injected with 25 μg/g of anti-CD4 by i.p. on P5, P13, and P36. Mice were analyzed at 8 weeks of age. **B, C** BTBR αCD4 mice had reduced frequency (**B**) and cell number (**C**) of brain-resident CD4⁺ T cells. CD8⁺ T cell frequency was increased (**B**), but not its absolute number (**C**). BTBR Ctrl $n = 3$ mice, BTBR αCD4 $n = 5$ mice. P value from two-tailed Student's t-test, $t(6) = 5.437$ and $t(6) = 4.701$ (**B**) and $t(6) = 4.719$ and $t(6) = 0.9473$ (**C**). **D, E** Time spent in chambers during the three-chamber sociability (**D**) and social novelty (**E**) tests. BTBR αCD4 sociability $P = 0.00009$, P value from two-way ANOVA, $F_{1,40} = 2.590$ and $F_{1,40} = 12.42$, respectively. BTBR Ctrl $n = 9$, BTBR αCD4 $n = 13$. **F** Percent of marbles buried during the marble burying test. P value from two-tailed Welch's t-test, $t(28.30) = 3.929$. BTBR Ctrl $n = 16$, BTBR αCD4 $n = 15$. **G, H** Time spent in the center zone (**G**) and mean velocity (**H**) during the open field maze. BTBR Ctrl $n = 14$, BTBR αCD4 $n = 13$. P value from two-tailed Welch's t-test, $t(23.52) = 3.077$ and $t(24.98) = 2.402$, respectively. **I, J** Representative flow cytometry plots, frequencies (**I**) and absolute cell numbers (**J**) of microglia and macrophages from live cells of the brain parenchyma. BTBR Ctrl $n = 3$ mice, BTBR αCD4 $n = 5$ mice. P values from two-tailed Student's t-test, $t(6) = 6.006$ and $t(6) = 1.733$ (**I**) and $t(6) = 3.458$ and $t(6) = 0.6370$ (**J**). **K–N** Representative flow cytometry plots and frequencies of IL-10⁺ (**K**), IL-6⁺ (**L**), TNF-α⁺ (**M**), and IL-1β⁺ (**N**) microglia. BTBR Ctrl $n = 3$ mice, BTBR αCD4 $n = 5$ mice. P values from two-tailed Student's t-test, $t(6) = 2.752$ (**K**), $t(6) = 4.726$ (**L**), $t(6) = 3.538$ (**M**), $t(6) = 0.5021$ (**N**). Flow cytometric analyses are representative results from at least 2 independent experiments with minimum of 3 mice. All data represented as mean ± SEM. Source data are available in source data file.

number of macrophages (Fig. 3I, J). Interestingly, the absence of CD4⁺ T cells influenced microglial phenotypes, reducing inflammatory M1 microglia while promoting a shift towards anti-inflammatory and tissue-repair-associated M2 microglia (Supplementary Fig. 5G). Moreover, the production of IL-10, IL-6, and TNF-α, but not IL-1β, were reduced in these microglia, highlighting a link between microglial function and CD4⁺ T cell presence in the brain. (Fig. 3K–N). These results suggest that brain-resident CD4⁺ T cells in BTBR mice may play a dual role, both contributing to neuroinflammation and regulating microglial function.

L. murinus and ASD-associated metabolites drive ASD pathology in BTBR mice

The abrogation of several ASD-associated behaviors and the regulation of brain-resident T cells in GF BTBR mice indicate that certain gut microbes may drive ASD in this model. To narrow down these microbes, we employed a microbiota depletion strategy utilizing different combinations of antibiotics consisting of ampicillin (A), vancomycin (V), neomycin (N), and metronidazole (M) in pregnant SPF BTBR mice (Fig. 4A). To streamline this experiment, the marble burying test for repetitive behavior was utilized as a diagnosis for ASD phenotype. Most of the antibiotic combinations successfully prevented repetitive behavior in BTBR mice, mirroring the phenotype of GF BTBR mice (Fig. 4B). However, mice treated with the VNM combination, which excludes ampicillin, did not show protection against repetitive behaviors (Fig. 4B). Ampicillin alone was also able to prevent repetitive behavior, suggesting that bacteria targeted by ampicillin might play a causative role for ASD in our model (Supplementary Fig. 6A). The observation was further supported by colonizing GF BTBR mice with feces derived from the VNM group, which recapitulated high repetitive behavior (Supplementary Fig. 6B, C). To identify the specific bacteria, we performed 16S rRNA sequencing and found that *Escherichia/Shigella* and *Lactobacillus* genera were highly enriched in the VNM microbiome (Fig. 4C). Our finding aligns with previous microbiome analyses of ASD patients, which show enrichment of the *Lactobacillus* genus compared to neurotypical individuals[3,32]. Targeted metabolomics was performed to identify gut microbiota-derived metabolites enriched in the VNM group. Several metabolites, including glutamate (Glu), 3-hydroxyglutaric acid (Oh-GlutAcid), histamine, putrescine, homocysteine (HCys), and lactic acid (Lac), were highly abundant in the VNM feces compared to the AVNM group (Fig. 4D). Notably, glutamate, an excitatory neurotransmitter associated with ASD, was enriched (Fig. 4E). While GABA levels were similar, the glutamate/GABA ratio in the feces showed a significant increase in the VNM group (Supplementary Fig. 6D, Fig. 4F). Our data supports clinical studies in which higher glutamate and lower GABA concentrations are found in ASD patients' feces, suggesting an excitatory/inhibitory imbalance in ASD[33,34]. Interestingly, 3-hydroxyglutaric acid, a neurotoxin associated with glutaric acidemia type 1, was also highly enriched in the ASD microbiota (Fig. 4G). This metabolite has been previously implicated in numerous behavioral and cognitive deficits, partly by inducing a glutamatergic and GABAergic imbalance[35,36].

To further specify the ASD-associated microbe, we performed several rounds of colony picking from the VNM feces and luminal content to isolate single bacterial colonies. We targeted *Lactobacillus* species, as they are also commonly elevated in ASD patients. Additionally, *Lactobacillus* was favored over *Escherichia/Shigella* species to avoid potential pathogenic properties upon mono-association into GF mice. Single colony picking under *Lactobacillus* enrichment conditions and 16S rRNA sequencing resulted in the identification of *L. murinus*, which composed the majority of single colonies (Fig. 4H). Furthermore, prior studies and genome assessments suggest the glutamate-producing capacity of *L. murnius* strains, supporting its pathogenic potential in BTBR mice[37]. We colonized 1×10^9 CFU/mouse of *L. murinus* by oral gavage into pregnant GF BTBR mice at E12.5 to determine whether this bacterium could recapitulate ASD phenotypes. *L. murinus* mono-association could indeed cause a significant increase in repetitive behavior compared to GF BTBR vehicle-treated mice (Fig. 4I). *L. murinus* colonization also impaired social memory during the three-chamber sociability and novelty test, mirroring SPF BTBR social phenotype (Supplementary Fig. 6E, F). To determine whether the recapitulation of ASD-associated behaviors was due to the general presence of microbiota or partial to *L. murinus*, we mono-associated another bacterium, *Bifidobacterium bifidum* into GF BTBR mice. However, *B. bifidum* was unable to induce repetitive behavior in GF BTBR mice, indicating that the recapitulation of repetitive behavior is specific to *L. murinus* (Supplementary Fig. 6G). Additionally, to test whether live bacteria was required, we treated heat-killed (H.K.) *L. murinus* into GF BTBR mice. H.K. *L. murinus* failed to induce repetitive behavior during the marble burying test, indicating that colonization of live bacteria was needed (Supplementary Fig. 6H). This suggests that metabolites from live bacteria may drive ASD in BTBR mice. Indeed, targeted metabolomics revealed that *L. murinus* elevated glutamate levels while reducing GABA levels in the guts of GF BTBR mice (Fig. 4J, Supplementary Fig. 6I). Likewise, *L. murinus* monoassociation increased the glutamate/GABA ratio and 3-hydroxyglutaric acid levels relative to GF BTBR (Fig. 4K, L). Finally, *L. murinus* monoassociation increased the production of IFN-γ in CD4⁺ and CD8⁺ T cells within the brain (Fig. 4M, N). These data suggest that *L. murinus* in the context of BTBR mice is sufficient to drive ASD-associated behavior and neuroinflammation.

Healthy gut microbiota promotes neurotypical behaviors and restrains neuroinflammation

Given the evidence that gut microbiota and their metabolites drive ASD phenotypes, we explored whether transferring a healthy gut microbiota could promote neurotypical behaviors in BTBR mice. We cohoused 3-weeks-old GF BTBR pups with SPF B6 or SPF BTBR mice, facilitating the transfer of gut microbiota (Fig. 5A). At 8 weeks of age, GF BTBR mice colonized with SPF B6 microbiota (BTBR-B6) exhibited neurotypical social behavior during the three-chamber sociability
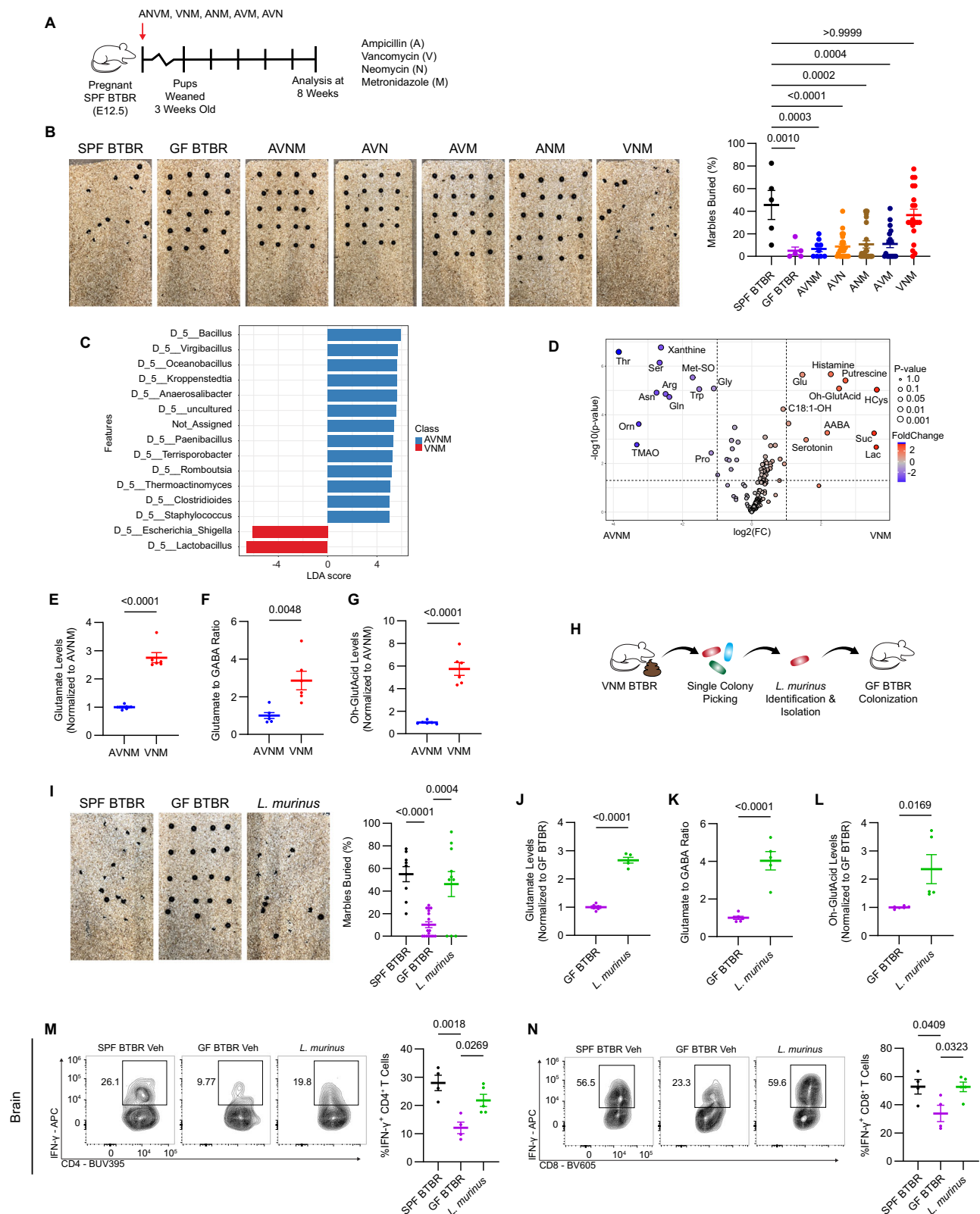
assay, while mice colonized with SPF BTBR microbiota (BTBR-BTBR) remained non-social (Fig. 5B). Likewise, the B6 microbiota conferred neurotypical social memory and reduced repetitive behavior in these BTBR mice (Fig. 5C, D). These behavioral changes were consistent with reduced c-FOS⁺ neurons in the amygdala and dentate gyrus in the BTBR-B6 group compared to the BTBR-BTBR group (Fig. 5E–G). To check whether this effect was dependent on postnatal or prenatal

intervention periods, we also performed microbiota transfer experiments on pregnant GF BTBR mice on embryonic day 12.5 (E12.5) (Supplementary Fig. 7A). When pups had matured to 8 weeks of age, they displayed similar behavioral changes as in the postnatal model, with improved sociability and reduced repetitive behavior (Supplementary Fig. 7B, C). Thus, our results indicate that healthy gut microbiota can protect from ASD-associated behaviors in BTBR mice.

Fig. 4 | Identification of gut microbiota and metabolites that drive ASD in BTBR mice. A Schematic for antibiotic treatment. **B** Representative images and percent of marbles buried. SPF and GF BTBR $n = 5$, AVNM $n = 9$, AVN $n = 22$, ANM $n = 25$, AVM $n = 17$ VNM $n = 20$. SPF BTBR vs AVN $P = 0.00008$, P values from one-way ANOVA with Bonferroni's correction, $F_{6,96} = 10.42$. **C** Linear discriminant analysis Effect Size (LEfSe) for genera enriched in AVNM or VNM groups. Genera with FDR-adjusted P value cutoff of 0.01 and Log LDA > 2.0 shown. **D** Volcano plot of fecal metabolites enriched in AVNM or VNM mice. Fold change threshold of 2.0 with two-tailed raw P value threshold of 0.05 from unpaired analysis with equal group variances. Significant metabolites labeled. **E–G** Relative glutamate (**E**), glutamate to GABA ratio (**F**), and 3-hydroxyglutaric acid (OH-GlutAcid) (**G**) levels in the feces normalized to AVNM. $n = 6$ mice. $P = 0.000002$ (**E**) and $P = 0.000008$ (**G**). P values from two-tailed Student's t-test, $t(10) = 9.627$ (**E**), $t(10) = 3.611$ (**F**),

$t(10) = 8.325$ (**G**). **H** Schematic of *L. murinus* isolation and monoassociation. **I** Representative images and percent of marbles buried. SPF BTBR $n = 9$, GF BTBR $n = 18$, GF BTBR + *L. murinus* $n = 10$. SPF BTBR vs GF BTBR $P = 0.00003$. P values from one-way ANOVA with Bonferroni's correction, $F_{2,34} = 15.97$. **J–L** Relative glutamate (**J**), glutamate to GABA ratio (**K**), and 3-hydroxyglutaric acid (**L**) levels in feces after *L. murinus* monoassociation. GF BTBR $n = 6$ mice, *L. murinus* $n = 5$ mice. $P = 0.00000005$ (**J**), $P = 0.00008$ (**K**). P values from two-tailed Student's t-test, $t(9) = 16.37$ (**J**), $t(9) = 6.768$ (**K**), $t(9) = 2.924$ (**L**). **M, N** Representative flow cytometry plots and frequencies of IFN-γ⁺ Foxp3⁻ CD4⁺ (**M**) and IFN-γ⁺ CD8⁺ (**N**) T cells in the brain after *L. murinus* monoassociation. SPF and GF BTBR $n = 4$ mice, *L. murinus* $n = 5$ mice. P values from one-way ANOVA with Bonferroni's correction, $F_{2,10} = 11.02$ (**M**), $F_{2,10} = 5.215$ (**N**). All data represented as mean ± SEM. Source data are available in source data file.

To further investigate the mechanisms underlying the protective role of B6 microbiota, we examined whether B6 microbiota could suppress neuroinflammation in BTBR mice. No significant changes were observed in the frequencies of brain-resident CD4⁺ or CD8⁺ T cells following microbiota transfer (Supplementary Fig. 7D). However, transfer of B6 microbiota increased the number of Tregs within the brain (Supplementary Fig. 7E, F). This was accompanied by a reduction in IFN-γ levels produced by brain-resident CD4⁺ and CD8⁺ T cells (Fig. 5H, I). Furthermore, the transfer of healthy gut microbiota elevated microglia populations in the brain (Fig. 5J, Supplementary Fig. 7G). These microglia exhibited increased IL-10 levels (Fig. 5K) and reduced production of pro-inflammatory cytokines, including IL-6, IL-1β, and a tendency for TNF-α (Fig. 5L–N). These phenotypic changes in BTBR-B6 and BTBR-BTBR microglia parallel the differences found between B6 and BTBR mice, suggesting that the gut microbiota may dictate neuroimmune phenotypes regardless of host genetics (Supplementary Fig. 7H–M).

Healthy gut microbiota reduces ASD-associated metabolites in BTBR mice

Our data shows that B6 microbiota in GF BTBR mice improved both social memory and sociability (Fig. 5B, C). In contrast, the absence of gut microbiota only enhanced social memory but not sociability in GF BTBR mice (Fig. 1A, B). This difference indicates that gut microbial dysbiosis and the enrichment of harmful microbes, including *L. murinus*, may impair social memory, while certain beneficial microbes and their metabolites are necessary for neurotypical sociability. To investigate the microbes and metabolites that promote neurotypical behaviors in BTBR-B6 mice, 16S rRNA sequencing was conducted. Beta diversity analysis revealed distinct clustering in the gut microbiota of BTBR-B6 mice (Fig. 6A). Particularly, several genera, including *Lachnospiraceae, Mucispirillum, Jeotgalicoccus*, and *Akkermansia* were enriched by healthy B6 microbiota (Fig. 6B). Among them, *Lachnospiraceae, Akkermansia, Bilophila, Tyhzzerella, Gemella,* and *Staphylococcus* have been reported to be elevated in neurotypical individuals compared to ASD patients[3]. Targeted metabolomics revealed that BTBR microbiota produced higher levels of glutamate and 3-hydroxyglutaric acid. In contrast, BTBR-B6 mice had increased levels of taurine and putrescine (Fig. 6C) and significantly reduced relative levels of glutamate and 3-hydroxyglutaric acid, with a tendency for reduced glutamate/GABA ratio (Fig. 6D–F). Taken together, these findings suggest that a healthy gut microbiota can alter the metabolite pool to mitigate the excitatory/inhibitory metabolic imbalance and suppress neuroinflammation, thereby protecting BTBR mice from ASD-associated behaviors.

Administration of probiotic *L. reuteri* IMB015 improves ASD-associated behaviors

To replicate the protective function of a healthy microbiota using a single defined bacterium, we conducted in silico analyses to identify bacterial strains capable of producing high levels of GABA and reducing glutamate, thereby lowering the glutamate/GABA ratio. To this

end, we performed genome-scale metabolic reconstructions, which recovers all metabolic reactions based on the bacterial genome, followed by flux-balance analyses with minimization of total flux to predict the metabolites produced or taken up by the bacteria[38] (Fig. 7A). This genome-based metabolic modeling approach facilitates the effective identification of candidate bacteria based on their metabolic capabilities. Among a cohort of tested probiotic candidate strains, we identified *L. reuteri* IMB015 (IMB015), which exhibited high GABA production and glutamate uptake (Fig. 7B). To assess the therapeutic potential of IMB015, we administered 1×10^9 CFU of IMB015 per mouse daily to SPF BTBR pups by oral gavage from 3 to 8 weeks of age (Fig. 7C). Both vehicle- (PBS) and IMB015-treated groups displayed impaired sociability during the three-chamber sociability assay (Fig. 7D). However, IMB015 treatment significantly improved social memory (Fig. 7E). Additionally, IMB015 protected BTBR mice from repetitive behavior during the marble burying test (Fig. 7F). While locomotor activity remained unchanged, IMB015 treatment reduced the center zone duration during the open field maze test (Fig. 7G, H). These behavioral normalizations were associated with changes in c-FOS levels in neurons, with IMB015 treatment significantly reducing neuronal hyperactivation in both the amygdala and the dentate gyrus of the hippocampus (Fig. 7I–K).

We performed a targeted metabolomic analysis to test whether the behavioral improvements of IMB015 are mediated by alterations in the glutamate/GABA ratio. Relative GABA levels showed a tendency to be elevated following IMB015 treatment, although it was not statistically significant (Supplementary Fig. 8A). Moreover, IMB015 treatment significantly reduced glutamate levels and the glutamate/GABA ratio (Fig. 7L, M). Additionally, IMB015 demonstrated a strong tendency to lower 3-hydroxyglutaric acid levels (Fig. 7N). In contrast to IMB015, harmful *L. murinus* had markedly elevated glutamate and 3-hydroxyglutaric acid levels (Fig. 4J–L). This dichotomy suggests that different species within even the same genus can differentially impact the metabolite pool and corresponding behaviors.

We then investigated whether the therapeutic effects of IMB015 were mediated through immune modulation. IMB015 administration induced anti-inflammatory phenotypes in the periphery, with an increase of Tregs in the small intestinal lamina propria and a decrease of IFN-γ production from splenic CD4⁺ and CD8⁺ T cells (Supplementary Fig. 8B–D). Similarly, IMB015 treatment elevated Treg cell numbers in the brains of BTBR mice (Fig. 7O) and reduced IFN-γ production from both CD4⁺ and CD8⁺ brain-resident T cells (Fig. 7P, Q). Although IMB015 treatment did not affect the production of IL-10, TNF-α, or IL-1β in microglia, it did reduce the population of IL-6⁺ microglia (Supplementary Fig. 8E–H). These results demonstrate the therapeutic potential of IMB015 to improve ASD-associated behaviors by altering the metabolite pool and modulating neuroinflammation.

Discussion
Recent studies in ASD emphasize that, although genetic predisposition enhances ASD susceptibility, non-genetic factors also substantially
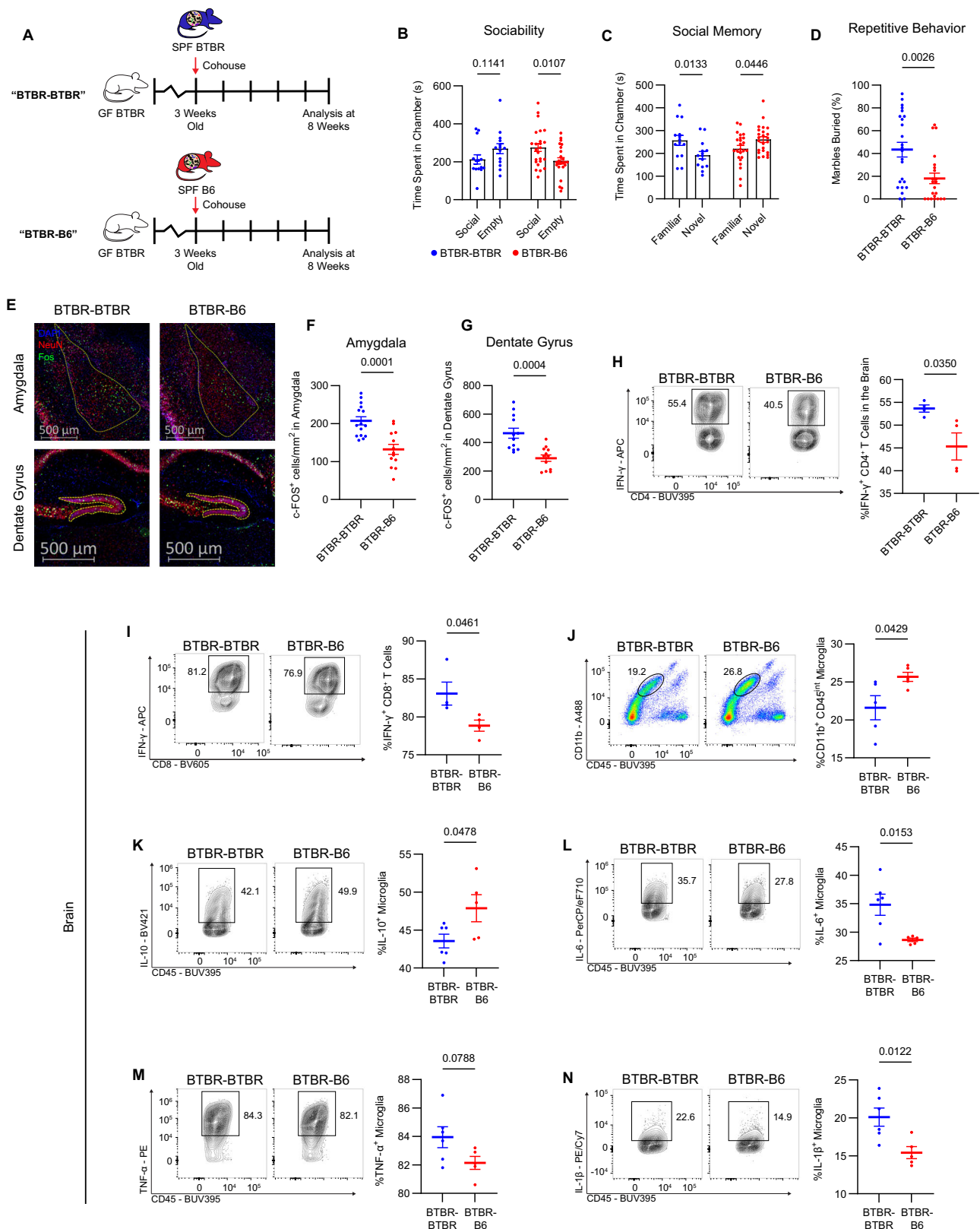
influence the manifestation and progression of specific phenotypes within the disorder. For this reason, we sought to delineate the gut-immune-brain axis in the context of genetic susceptibility to ASD. By employing the BTBR mouse model, we revealed several critical findings in this study: (1) gut microbiota regulates ASD phenotypes and neuroinflammation by regulating brain-resident T cells and microglia populations; (2) CD4+ T cells drive ASD pathogenesis; (3) *L. murinus* is

capable of inducing ASD-like behaviors through the upregulation of the glutamate/GABA ratio and neurotoxic 3-hydroxyglutaric acid; and (4) beneficial gut microbiota, derived from B6 mice or the probiotic strain *L. reuteri* IMB015, alleviates ASD phenotypes by reducing pathogenic metabolites and suppressing neuroinflammation. These findings suggest that the gut microbiota and its interaction with the host immunity can supersede genetic predisposition behind ASD.

Fig. 5 | Healthy B6 microbiota confers neurotypical behavior and neuroimmune modulation in BTBR mice. A 3-weeks-old GF BTBR pups were cohoused with either SPF B6 (BTBR-B6) or SPF BTBR (BTBR-BTBR) mice. **B, C** Duration in chambers during the sociability (**B**) and social novelty (**C**) tests. BTBR-BTBR $n = 14$, BTBR-B6 $n = 24$, P values from two-way ANOVA, $F_{1,72} = 8.186$ (**B**), $F_{1,72} = 10.61$ (**C**). **D** Percent of marbles buried. BTBR-BTBR $n = 24$, BTBR-B6 $n = 22$, P value from two-tailed Welch's t-test, $t(40.98) = 3.213$. **E−G** Representative immunofluorescence staining and number of c-FOS⁺ neurons per area in the amygdala (**F**) and dentate gyrus (**G**). P value from two-tailed Student's t-test, $t(26) = 4.445$, BTBR-BTBR $n = 15$ sections, 5 mice, BTBR-B6 $n = 13$ sections, 5 mice (**F**). $t(22) = 4.180$, BTBR-BTBR $n = 12$ sections, 5 mice, BTBR-B6 $n = 12$ sections, 5 mice (**G**). **H, I**

Representative flow cytometry plots and frequencies of IFN-γ⁺ Foxp3⁻ CD4⁺ (**H**) or IFN-γ⁺ CD8⁺ (**I**) T cells in the brain. BTBR-BTBR and BTBR-B6 $n = 4$ mice, P value from two-tailed Student's t-test, $t(6) = 2.711$ (**H**), $t(6) = 2.507$ (**I**). **J** Representative flow cytometry plots and frequencies of CD11b⁺ CD45^{int} microglia in the brain. BTBR-BTBR and BTBR-B6 $n = 5$ mice, P values from two-tailed Student's t-test, $t(8) = 2.404$. **K−N** Representative flow cytometry plots and frequencies of IL-10⁺ (**K**), IL-6⁺ (**L**), TNF-α⁺ (**M**), or IL-1β⁺ (**N**) microglia in the brain. BTBR-BTBR $n = 6$ mice, BTBR-B6 $n = 5$ mice. P values from two-tailed Student's t-test, $t(9) = 2.289$ (**K**), $t(9) = 2.988$ (**L**), $t(9) = 1.982$ (**M**), $t(9) = 3.125$ (**N**). Flow cytometry data are representative of at least 2 independent experiments with minimum 3 mice. All data represented as mean ± SEM. Source data are available in source data file.
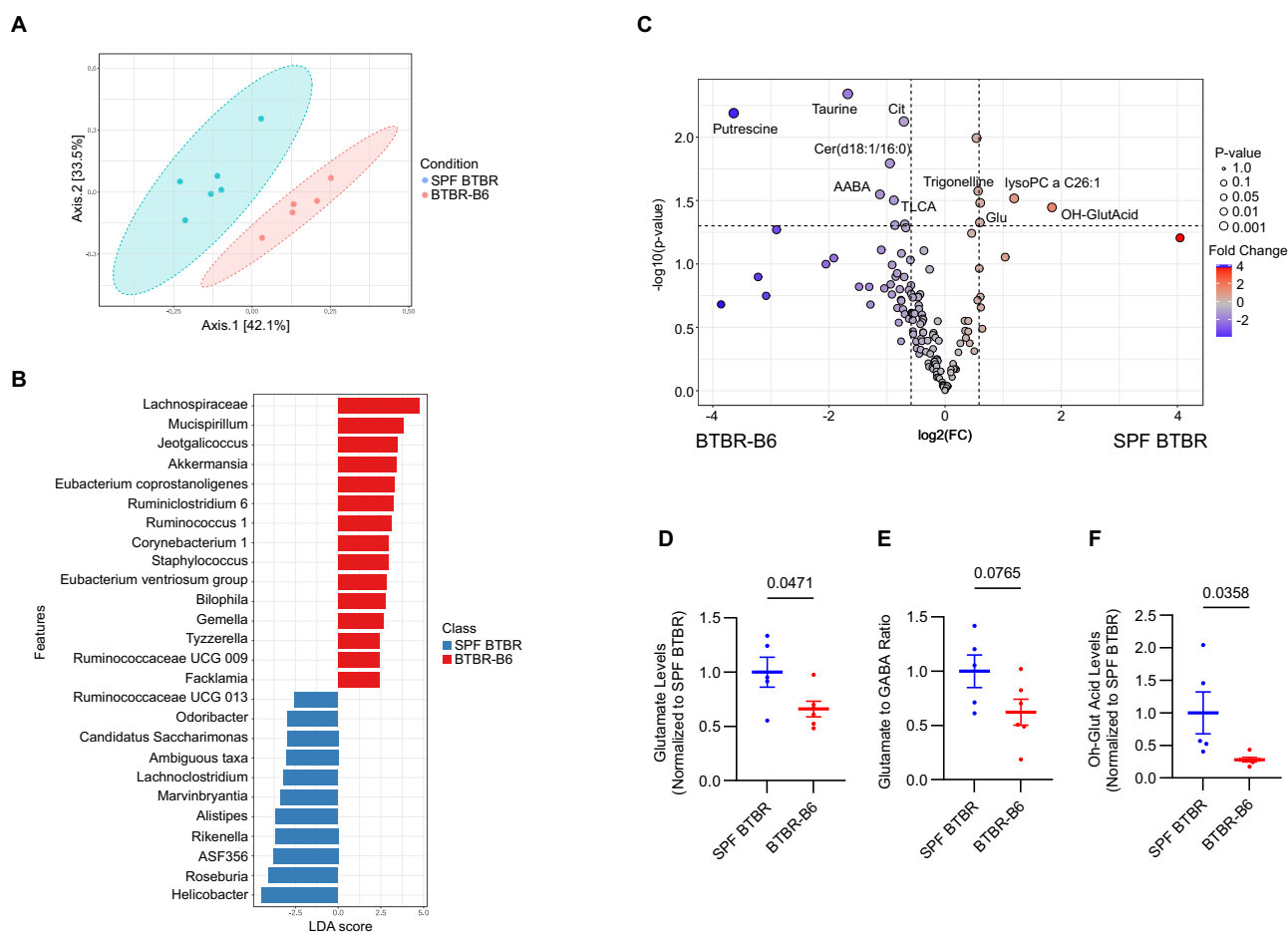

Fig. 6 | Healthy gut microbiota reduces ASD-associated metabolites in BTBR mice. A Beta diversity from Principal coordinates analysis (PCoA) based on Bray-Curtis dissimilarity index demonstrating a unique microbiota composition following colonization with healthy gut microbiota from B6 mice (Pairwise PERMANOVA, $F = 5.61$, $R^2 = 0.38$, $P = 0.004$). **B** LEfSe analysis of genera enriched in SPF BTBR or B6 microbiota recipient BTBR (BTBR-B6) mice. Genera with FDR-adjusted P value cutoff of 0.1 and Log LDA > 2.0 shown. **C** Volcano plot of fecal metabolites enriched in SPF BTBR or BTBR-B6 mice. Fold change threshold of 1.5 with two-tailed raw P value threshold of 0.05 from unpaired analysis with equal group variances. All significant metabolites labeled. **D−F** Relative glutamate (**D**), glutamate to GABA ratio (**E**), and 3-hydroxyglutaric acid (**F**) levels in feces after colonization with healthy gut microbiota. SPF BTBR $n = 5$, BTBR-B6 $n = 6$. P values from two-tailed Student's t-test, $t(9) = 2.299$ (**D**), $t(9) = 2.000$ (**E**), $t(9) = 2.466$ (**F**). All data represented as mean ± SEM. Source data are available in source data file.

A previous study using the *Cntnap2$^{-/-}$* mice demonstrated that hyperactivity is attributed to host genetics, whereas sociability and social memory are linked to the gut microbiota and its metabolites[4]. More specifically, heterozygous breeding between wildtype and *Cntnap2* knockout (KO) mice resulted in KO littermates with a unique microbiota composition, neurotypical social behavior, and ASD-associated hyperlocomotion[4]. These phenotypes could be recapitulated by cohousing[4]. Our findings align with this concept and provide additional insights. Under the BTBR genetic background, GF status did not affect sociability or hyperactivity, but significantly normalized

social memory, repetitive behavior, and anxiety-like behavior. Notably, the absence of gut microbiota reduced the population of proinflammatory brain-resident CD4⁺ T cells, highlighting a gut-immune-brain axis in this model. This observation is consistent with prior research indicating that gut microbiota can peripherally activate conventional CD4⁺ T cells, enabling their migration into the brain, where they interact with microglia[27]. While the depletion of gut microbiota or CD4⁺ T cells improved some ASD-associated behaviors, sociability was only restored by transferring healthy B6 microbiota into GF BTBR mice. This suggests that sociability may rely on a distinct axis involving
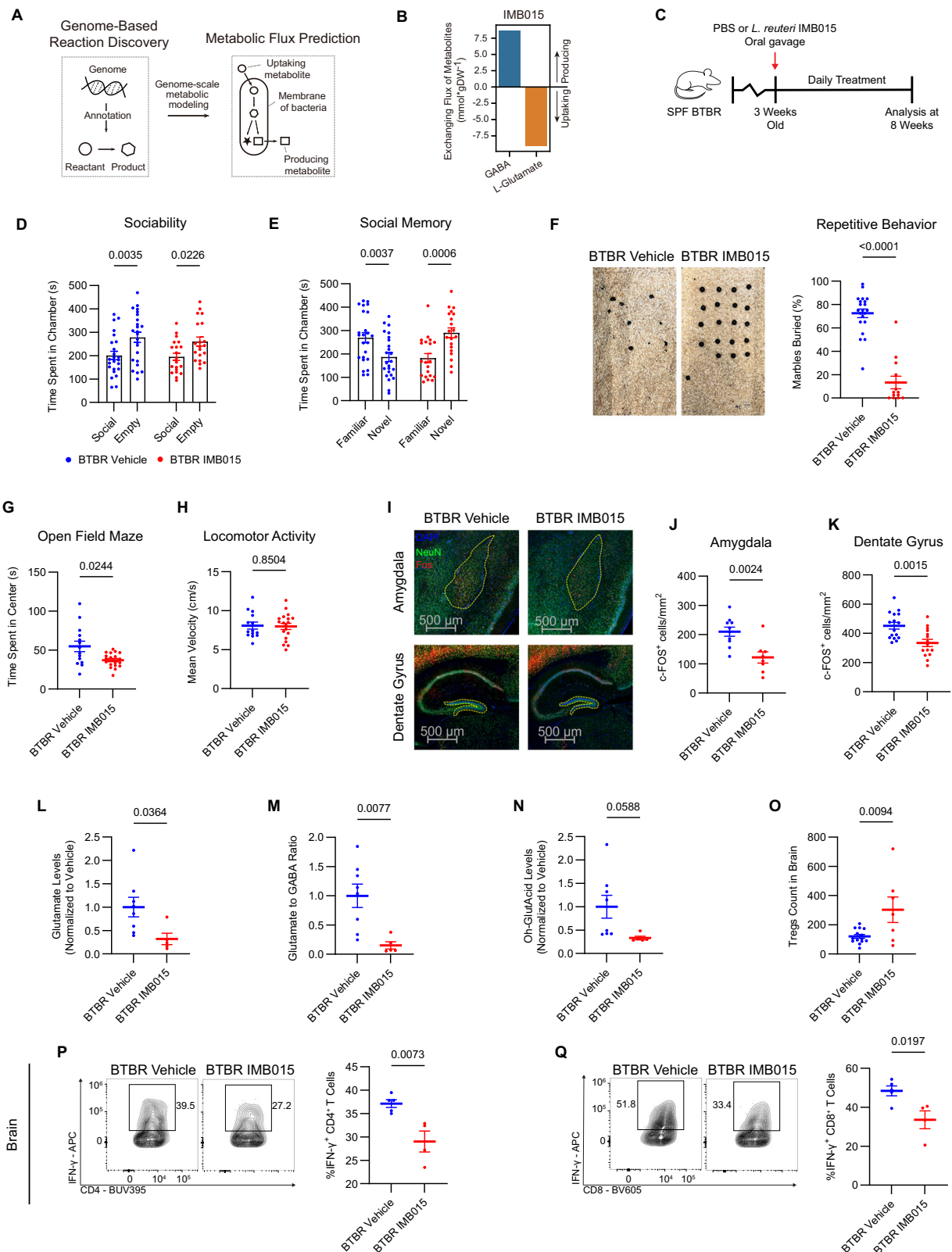
specific healthy gut microbes and their metabolites. Together, our findings highlight the multifaceted and behavior-specific mechanisms underlying the gut-immune-brain connection in ASD.

The phenotype of GF BTBR mice suggested that harmful bacteria may drive ASD in SPF BTBR mice. The use of antibiotic combinations revealed that ampicillin-sensitive bacteria were capable of recapitulating ASD symptoms. Through 16S rRNA sequencing, we identified

Lactobacillus and *Escherichia/Shigella* genera, both of which are commonly elevated among ASD patients[39,40]. We demonstrate that the monoassociation of GF BTBR mice with *L. murinus* could induce repetitive behavior and T cell-mediated neuroinflammation. *Lactobacillus* is a large genus encompassing species and strains with vast functional properties. For instance, distinct strains within the same *L. plantarum* species can exhibit opposing immunological effects, having

Fig. 7 | *L. reuteri* IMB015 therapeutically alleviates ASD-associated phenotypes. **A** Schematic diagram of in silico metabolic flux prediction. **B** Predicted GABA and L-glutamate production or uptake in IMB015. **C** Schematic diagram of IMB015 treatment. **D, E** Time spent in chambers during the sociability (**D**) and social novelty (**E**) tests. BTBR Vehicle $n = 24$, BTBR IMB015 $n = 20$, P values from two-way ANOVA, $F_{1,84} = 0.096673$ (**D**), $F_{1,84} = 21.67$ (**E**). **F** Representative images and percentage of marbles buried. BTBR Vehicle $n = 21$, BTBR IMB015 $n = 13$. $P = 0.000000005$. P value from two-tailed Welch's t-test, $t(22.62) = 9.059$. **G, H** Time spent in the center zone (**G**) and mean velocity (**H**) during the open field maze. BTBR Vehicle $n = 14$, BTBR IMB015 $n = 19$. P value from two-tailed Welch's t-test, $t(15.43) = 2.494$ (**G**), $t(28.60) = 0.190$ (**H**). **I–K** Representative immunofluorescence staining and number of c-FOS^{+} neurons per area in the amygdala (two-tailed Student's t-test, $t(16) = 3.593$. BTBR Vehicle $n = 10$ sections, 3 mice, BTBR IMB015 $n = 8$ sections, 4 mice) and

dentate gyrus ($t(29) = 3.504$. BTBR Vehicle $n = 16$ sections, 3 mice, BTBR IMB015 $n = 15$ sections, 3 mice). **L–N** Relative glutamate (**L**), glutamate/GABA ratio (**M**), and Oh-GlutAcid (**N**) levels in feces after IMB015 treatment. BTBR Vehicle $n = 8$, BTBR IMB015 $n = 5$. P values from two-tailed Student's t-test, $t(11) = 2.382$ (**L**), $t(11) = 3.252$ (**M**), $t(11) = 2.108$ (**N**). **O** Absolute cell count of Tregs in the brain from flow cytometry. BTBR Vehicle $n = 14$, BTBR IMB015 $n = 7$. P value from two-tailed Student's t-test, $t(19) = 2.891$. **P, Q** Representative flow cytometry plots and frequencies of IFN-γ^+ Foxp3$^-$ CD4$^+$ (**P**) or IFN-γ^+ CD8$^+$ (**Q**) T cells in the brain. BTBR Vehicle $n = 5$ mice, BTBR IMB015 $n = 4$ mice. P value from two-tailed Student's t-test, $t(7) = 3.741$ (**P**), $t(7) = 3.010$ (**Q**). Flow cytometry data from 2 independent experiments with minimum 3 mice. Data represented as mean ± SEM. Source data are available in source data file.

either pro- or anti-inflammatory capabilities. In mice, *L. plantarum* IMB19 can elevate IFN-γ, while *L. plantarum* OLL2712 can induce high IL-10 production[41,42]. In this manner, while often regarded as an anti-inflammatory probiotic, certain *Lactobacillus* species and strains can exhibit pro-inflammatory effects and contribute to disease pathology. This duality may explain how *L. murinus* can drive ASD, whereas another *Lactobacillus*, *L. reuteri* IMB015, confers therapeutic potential.

In this study, we identified glutamate and GABA pathways as potential metabolic drivers for ASD. Disruptions in the balance between excitatory and inhibitory neurotransmitters, specifically within the glutamatergic and GABAergic systems, are well-recognized as crucial contributors to ASD[43]. ASD patients exhibit elevated glutamate levels in the blood, brain, and urine, along with reduced levels of GABA, further underscoring the relevance of these pathways in the disorder[44–46]. Alongside glutamate, we identified 3-hydroxyglutaric acid, a neurotoxin and byproduct of tryptophan, lysine, and hydroxylysine metabolism, as another potential contributor to ASD. Glutaric acidemia type 1, a metabolic disorder caused by a deficiency in glutaryl-CoA dehydrogenase, leads to the accumulation of glutaric acid and 3-hydroxyglutaric acid, resulting in neurological abnormalities[35]. Notably, 3-hydroxyglutaric acid disrupts glutamate decarboxylase, preventing GABA synthesis, and thereby disrupting the glutamatergic and GABAergic balance[36].

Along with several ASD-associated metabolic and microbial markers, we also identified microbes and metabolites that may protect BTBR mice from ASD. In GF BTBR mice harboring B6 microbiota, *Lachnospiraceae*, *Akkermansia*, and *Tyzzerella* genera were enriched, which are also more abundant in neurotypical individuals compared to ASD patients[47,48]. Putrescine and taurine were also enriched by B6 microbiota, with taurine specifically having previously been shown to improve behaviors in BTBR mice[2]. Further studies are required to specify which strains are beneficial, and whether these metabolites are directly produced by them.

LBPs are garnering high interest as potential therapeutics for ASD. *L. reuteri* strains are widely studied in animal and clinical studies, with numerous studies demonstrating their efficacy in successfully modifying behavior[4,6,8]. *L. reuteri* MM4-1A (ATCC-PTA-6475) and *L. reuteri* C501 significantly improves sociability, social memory, and repetitive behaviors across various mouse models[4,6,49]. For instance, neurotypical sociability could be induced by *L. reuteri* MM4-1A in the *Shank3B*$^{-/-}$ mouse model for ASD[5]. *Shank3B*$^{-/-}$ mice show gut microbial dysbiosis, including a decreased *L. reuteri* abundance. *L. reuteri* MM4-1A treatment could offset this difference and also elevate oxytocin levels, resulting in improved behavior[5]. In humans, combined administration of *L. reuteri* MM4-1A and DSM-179938 improved broad social functioning in ASD patients, although it did not significantly affect overall disorder severity or repetitive behaviors[8].

Utilizing in silico metabolism prediction models based on bacterial genomes, we identified *L. reuteri* IMB015 as a probiotic candidate with a high glutamate/GABA flux potential. Administration of IMB015 to BTBR mice resulted in reduced fecal glutamate levels and a lowered glutamate/GABA ratio, accompanied by a decrease in 3-hydroxyglutaric acid levels. While IMB015 did not improve sociability, it significantly ameliorated social novelty recognition, repetitive behaviors, and anxiety-like behavior. Additionally, IMB015 suppressed proinflammatory signals in the brain, including IFN-γ^+ T cells and IL-6$^+$ microglia. These findings highlight the metabolic and immune-modulatory functions of IMB015, underscoring its therapeutic potential in ASD.

We acknowledge several limitations in our study. Firstly, our study utilized only one mouse model of ASD. Nonetheless, numerous publications suggest parallels across mouse models. For instance, antibiotic treatment in *Shank3*$^{-/-}$ mice was shown to exacerbate social behavior without affecting anxiety-like behavior[50]. Furthermore, both *Shank3*$^{-/-}$ and *Cntnap2*$^{-/-}$ models are characterized with inflammation, and have responded positively to *L. reuteri*-based therapeutics[4,5,51–53]. Future studies into the gut-immune-brain axis in more animal models will help establish robust mechanistic pathways in ASD with greater translational capacities.

Second, it is unclear whether brain-resident T cells regulate ASD in a region-specific manner. Generally, B6 mice have less than 2000 total CD4$^+$ T cells in the brain, and the degree of detection can vary across research groups[27]. Due to their small population, we were unable to specify whether brain-resident T cells elicit localized inflammation in specific brain regions, or whether they contribute to general neuroinflammation across the entire brain. Advanced single-cell analyses of brain-resident T cells and microglia in specific brain regions during ASD could provide further insights into these mechanisms.

Finally, while higher glutamate in the feces was correlated with ASD-associated behavior, it is undetermined whether glutamate levels were altered within the brains of BTBR mice. Glutamate enters the brain through glutamate transporters, and can even cause BBB permeability, so elevated systemic glutamate levels could be hypothesized to accumulate within the brain[44,54]. For instance, glutamate levels were reported to be elevated in both the blood and the brain of patients, suggesting that peripheral glutamate concentrations may parallel that of the brain[44]. Moreover, feeding poly-gamma-glutamate in rats result in elevated glutamate and GABA levels in both the serum and the brain, indicating that intestinal glutamate metabolism could directly be linked with its concentration in the brain[55]. Future studies comparing metabolite levels in the gut, serum, and brain may further elucidate the role of microbial metabolites in the gut-immune-brain etiology of ASD.

Methods

Animals

All mouse experiments were approved by the POSTECH Institutional Animal Care and Use Committee (POSTECH-2020-0110-R4). Mice were maintained under SPF or GF conditions in sterile flexible film isolators (Class Biological Clean Ltd., USA) at the POSTECH Biotech Center animal facility. C57BL/6 (JAX: 000664; RRID:IMSR_JAX:000664) mice were purchased from Hyochang Science (Daegu, Korea) and

maintained at POSTECH. BTBR T^+ $Itpr3^{tf}$/J (BTBR) (JAX: 002282; RRI-D:IMSR_JAX:002282) mice were obtained from The Jackson Laboratory and maintained at POSTECH. GF BTBR mice were derived embryonic transfer and GF status was monitored monthly by culture of cecal and fecal contents, as well as PCR of bacterial 16S rRNA using universal primers[56]. Mice were housed under a 12-h light/dark cycle and food and water were available *ad libitum*. Diets were composed of Purina Lab Rodent Diet (100000 95135, Cargill Agri Purina) for SPF and Teklad Global 18% Protein Rodent Diet (2018S, Inotiv) for GF mice. Autoclaved aspen shaving bedding (L) (KOATECH) was used for all animals. Cages and water were changed on a weekly basis, unless otherwise specified for treatment groups. Ambient temperature and humidity was maintained at 20 °C and 60% humidity, respectively. All behavior, flow cytometry, imaging, and sequencing experiments were performed with male mice between 7 and 8 weeks old. Only male mice were used in this study for two reasons. Firstly, clinical evidence indicate ASD has a higher prevalence among males. We chose to use male mice to bridge more translational relevance in our study. Secondly, only one mouse sex was used for behavior studies to prevent any sexual bias that could alter mouse behaviors, particularly during social tests. Female mice were not tested in this study, and no data were collected using them. Mice were euthanized through the use of CO_2 and cervical dislocation. For analyses of the brain, mice were administered with mixtures of ketamine and xylazine (80 mg/kg i.p. and 10 mg/kg i.p., respectively) 20 min prior to perfusion of the heart with PBS and/or and 4% paraformaldehyde.

CD4$^+$ T cell depletion
CD4$^+$ T cells were depleted from BTBR mice by i.p. injection with 25 μg/g anti-CD4 (Cat. BP0003-1, Lot: 798421M1, Clone GK1.5, BioX-Cell) diluted in PBS at P5, P13, and P36[27]. Vehicle control mice were also injected at equivalent time points. CD4$^+$ T cell depletion was confirmed by flow cytometry analysis of the spleen, small intestines, and the brain at 8 weeks of age.

Targeted antibiotics treatment
Targeted antibiotics treatment to isolate ASD-phenotype-associated microbiota was performed by using combinations of ampicillin (Sigma-Aldrich) (1 g/l), vancomycin (Sigma) (0.5 g/l), neomycin (Sigma) (1 g/l), and metronidazole (ACROS Organics) (1 g/l), which were mixed and filtered[57]. Antibiotic combinations were administered in drinking water *ad libitum* in a concentration-dependent manner, and solutions were changed daily with new antibiotic mixtures as to maintain high active concentration peaks. Pregnant BTBR mice were treated from E12.5 until offspring were 8 weeks of age, and no significant weight change was observed in the groups. Mice were caged in groups of three to four and the amount of antibiotics consumed was monitored by averaging the amount of solution consumed daily in each cage.

Three-chamber sociability and novelty test
To assess mouse social preference and social memory, a modified three-chamber sociability and novelty test was performed[58]. Clear acrylic three-chamber sociability arenas of 60 × 40 × 22 (h) cm were used (SciTech Korea), and motion was assessed by EthoVision XT15 (Noldus). Male mice aged 7–8 weeks were used as subjects and male C57BL/6 mice of similar age and/or size were used as social and novel targets. Mice were first habituated in the center arena for 5 min. Then a full arena habituation was conducted for 10 min with the chamber doors open. Sociability test was then conducted for 10 min with one chamber containing a stranger C57BL/6 target mouse in a 10 cm diameter × 16 cm height wire cage (SciTech Korea) and the opposing chamber containing an empty wire cage. The positions of the wire cages were counterbalanced between trials to prevent environmental bias[4]. The social novelty test was performed for 10 min following the

sociability test. The empty wire cage from before was replaced with a cage containing a stranger C57BL/6 mouse in the opposing chamber, allowing the subject mouse to spend time with the familiar or novel mouse. Subject mice were isolated to the center chamber with the doors closed between the setup for sociability and novelty phases. Ethovision XT15 was used to measure the amount of time spent in either chamber based on the center point. The total time spent in either chamber was used to determine social and novel preferences. Neurotypical social preference was defined as more time spent in the social chamber, while ASD-associated non-social behavior was defined as either no preference between chambers or greater preference for the empty chamber. We defined neurotypical social memory as more time spent in the novel chamber, whereas impaired social memory was defined as no preference between chambers or more preference for the familiar chamber. All equipment was cleaned with 70% ethanol and fully dried before each experiment set.

Open field maze test
Anxiety-like and locomotor behaviors was measured using the Open Field Maze[59]. A 50 × 50 × 40 (h) cm opaque acrylic chamber was used to measure the motion of the subject mouse for 10 min. Mice were carefully placed in the center of the arena. EthoVision XT15 (Noldus) was used to calculate the frequency and amount of time spent within a center 17 cm × 17 cm region and the overall speed and distance traveled during the test. All equipment was cleaned with 70% ethanol and fully dried between each experiment set.

Marble burying test
The marble burying test was used to analyze mouse repetitive behavior[22,60]. A 26 × 47.6 × 20.3 (h) cm rat plastic cage (Perotech) was covered with fine Aspen Bedding 2 × 2 × 1 (h) mm (TAPVEI), and 20 marbles were placed in an orderly 4 × 5 arrangement. Mice were carefully placed at a designated landing zone at the bottom of the cage at the start of the experiment. Mice were tested for 15 min, following which, the number of marbles buried was calculated by independent observers who were blind to the treatment groups.

Isolation of immune cells for flow cytometric analysis
Immune cells were harvested from the spleen, lymph nodes, small intestines, colon, and the brain of mice. Mice were anesthetized with ketamine (80 mg/kg) and xylazine (10 mg/kg) prior to perfusion with 50 ml of cold 1x PBS. The spleen was dissociated with 70 μm strainers and red blood cells were lysed with 1x RBC lysis buffer (eBioscience). For the small intestines and colon, tissues were processed as previously described[61]. Briefly, the intestines were longitudinally cut, washed with PBS, and then cut into 0.5 cm pieces. Tissue were incubated in FACS buffer containing PBS with 10 mM EDTA, 20 mM HEPES, 1 mM sodium pyruvate, and 3% FBS while being stirred for 20 min at 37 °C. Intestinal and brain tissues were minced and incubated with RPMI 1640 media with 3% FBS, 20 mM HEPES, 1 mM sodium pyruvate, 0.5 mg/ml of Collagenase D (Roche), and DNase I (Sigma-Aldrich) for 45 min at 37 °C. Immune cells were isolated using a 30% and 70% Percoll™ (GE Healthcare) gradient and then washed with FACS buffer.

For cytokine analysis, PMA and Ionomycin (Calbiochem) as well as Golgi-Stop (BD Biosciences) were given for 4 h at 37 °C in RPMI media containing 10% FBS, 2 mM L-glutamine, 1 mM sodium pyruvate, 1 mM non-essential amino acids, 1% penicillin and streptomycin, and 0.1% β-ME (v/v). Cells were then stained with Fixable Viability Dye 1:1000 (Cat. 65-0866-18, Lot: 2010926, Invitrogen) and antibodies for surface markers. Cells were fixed and washed with Foxp3/Transcription Factor Fixation and Permeabilization Buffer (eBioscience), respectively, before being stained for intracellular molecules. Cells were washed with respective buffers between each step. The antibodies and their clones used are as follows: CD4 – BUV395; 1:400 (Cat. 563790, Lot: 3184615, Clone GK1.5, BD), CD8a – BV605; 1:400 (Cat. 100744, Lot:

B336700, Clone 53-6.7, Biolegend), CD45 – PerCP/Cy5.5; 1:400 (Cat. 103132, Lot: B295198, Clone 30-F11, Biolegend), TCRβ – APC/eF780; 1:200 (Cat. 47-5961-82, Lot: 2481347, Clone H57-597, Invitrogen), CD11b – A488; 1:400 (Cat. 101217, Lot: B307666, Clone M1/70, Biolegend), CD86 – BV605; 1:200 (Cat. 105037, Lot: B373866, Clone GL-1, Biolegend), CD206 – APC; 1:200 (Cat. 141708, Lot: B218214, Clone C068C2, Biolegend), Foxp3 – FITC; 1:200 (Cat. 11-5773-82, Lot: 2731698, Clone FJK-16a, Invitrogen), IFN-γ – APC; 1:100 (Cat. 17-7311-82, Lot: 2524225, Clone XMG1.2, Invitrogen), IL-1β – PE/Cy7; 1:100 (Cat. 25-7114-80, Lot: 2885871, Clone NJTEN3, Invitrogen), IL-10 – BV421; 1:100 (Cat. 505022, Lot: B375635, Clone JES5-16E3, Biolegend), IL-6 – PerCP/eF710; 1:100 (Cat. 46-7061-82, Lot: 2117496, Clone MP5-20F3, Invitrogen), TNFα – PE; 1:100 (Cat. 12-7321-82, Lot: 2473693, Clone MPX-XT22, Invitrogen). Cell acquisition was performed on the Beckman Coulter CytoFLEX S and analyzed using FlowJo v10.10 (Tree Star).

Isolation of *L. murinus*

Fresh feces from 8-week-old VNM-treated BTBR mice were homogenized in PBS and Lactobacilli were enriched using acidified Difco™ Lactobacilli MRS broth (BD) with 0.1% L-cysteine HCL for 2 h at 37 °C. 10-fold serial dilutions were made before being spread and grown on Difco™ Lactobacillii MRS Agar (BD) with 0.1% L-cysteine HCL and pH adjusted to 6.5 for 48 h at 37 °C. Single colonies were picked and streaked on MRS agar plates, and this process was repeated 3 times. Final single colonies were picked and inoculated in 5 ml MRS broth with 0.1%% L-cysteine HCL for 24 h at 37 °C before samples were analyzed by colony PCR using *Lactobacillus*-specific primers LbLMA1-rev (5′ CTC AAA ACT AAA CAA AGT TTC 3′) and R16-1 (5′ CTT GTA CAC ACC GCC CGT CA 3′)[62]. Colonies determined as *Lactobacillus* genus underwent 16S rRNA sequencing (Macrogen, Korea) using primers 785 F (5′ GGA TTA GAT ACC CTG GTA 3′) and 907 R (5′ CCG TCA ATT CMT TTR AGT TT 3′) and identified by matching against NCBI 16S database with BLAST (blastn). Results with over 99% sequence identities were tested in vivo.

Microbiota transfer experiment

GF BTBR mice were weaned at 3-weeks of age and removed from sterile flexible isolators and housed with either SPF BTBR or SPF C57BL/6 male mice in the SPF facility. To test prenatal microbiota transfer experiment, pregnant GF BTBR female mice were removed from their sterile flexible isolators at E12.5 and housed with either SPF BTBR or SPF C57BL/6 female mice in the SPF facility. Microbiota transfer was checked using PCR and gel electrophoresis of feces, as well as 16S rRNA sequencing (DNA Link, Korea). Behavior and immune analysis were performed when recipient mice grew to 8 weeks of age.

Prediction of metabolite production or uptake in bacteria using bacterial genome analysis

To predict metabolite production or uptake by a bacterial strain, a genome-scale metabolic reconstruction followed by flux balance analysis (FBA) with the minimization of total flux (MTF) was utilized. The reconstruction was carried out using gapseq (2024. 10. 30. committed version 8536a73, https://github.com/jotech/gapseq/tree/8536a73383bb902a25af6be7cf5f9f15a8e237c5). Protein sequences translated from the bacterial genome served as input, and the reconstruction was performed using the "doall" function with default settings.

FBA with MTF was then applied to the gap-filled reconstruction under a "gut" medium condition to predict the production or uptake of metabolites. To this end, the sybil R package (v. 2.2.0) was used. In the resulting flux profile, metabolites with an MTF flux greater than 0 in exchange reactions were classified as produced, while those with an MTF flux less than 0 were classified as uptake. Specific coding for this study are available at https://github.com/IMB-AI/JohnPark-ASD[63].

Bacteria treatment

L. reuteri IMB015 was cultured and provided by ImmunoBiome Inc. IMB015 was cultured in MRS broth (MBcell) for 16 h in glass bottles or 10 h in a fermenter (Sartorius) at 37 °C. Bacterial pellets were washed with DPBS and a 5% trehalose (w/v) solution was used as cryoprotectant before being frozen at -80 °C and lyophilized. Viable bacterial c.f.u. was measured using BactoBox (SBT Instruments) according to manufacturer's protocols.

L. murinus single colonies were cultured in MRS broth (BD) as described above. Bacterial concentrations were calculated and adjusted before treating GF BTBR mice with 1×10^9 CFU/mouse viable bacteria by oral gavage. Pregnant GF BTBR mice were colonized with *L. murinus* at E12.5. Control GF or SPF BTBR mice for the experiment were oral gavaged with DW at equivalent time points to eliminate any indirect effect from mouse handling. Successful colonization was confirmed in adult offspring by PCR of feces using *Lactobacilus* genus-specific PCR primers (5P-CTC AAA ACT AAA CAA AGT TTC-3P) and (5P-CTT GTA CAC ACC GCC CGT CA-3P). Heat-killed *L. murinus* was performed at 70 °C for 30 min, and GF BTBR mice were treated with H.K. *L. murinus* in the same manner as with the live bacteria.

Immunofluorescence staining

To analyze neuron activation following repetitive behavior, subject mice performed the marble burying test and were immediately anesthetized and sacrificed by cardiac perfusion with 1X PBS and 4% paraformaldehyde solution. Whole brains were isolated and placed in 30% sucrose (Sigma-Aldrich) solution for 12 h. Brains were embedded in O.C.T. compound (Sakura) and frozen at -80 °C. Brains were sectioned at 30 μm thicknesses and were washed in 1X PBST with 0.3% Triton X-100 (Sigma-Aldrich) for three times. Blocking was performed in 2% goat serum (Cat. 005-000-121, Lot: 146807, Jackson ImmunoResearch) before staining with primary and secondary antibodies for 12 h and 2 h, respectively. The following antibodies were used: rabbit anti-c-Fos 1:1000 (Cat. 226 008, Lot: 1-17, Clone Rb108B5, Synaptic Systems), guinea pig anti-NeuN 1:1000 (Cat. ABN90P, Lot: 4209899, Clone A60, Millipore), goat anti-rabbit Alexa Fluor 488 1:500 (Cat. 111-545-003, Lot: 164290, Polyclonal, Jackson ImmunoResearch), and donkey anti-guinea pig Cy3 1:500 (Cat. 706-165-148, Lot: 127715, Polyclonal, Jackson ImmunoResearch). Tissues were mounted with Vectashield with DAPI (H-1200-10, Vector Laboratories). Confocal imaging was conducted using an Axioscan Slide Scanner (Zeiss) and analysis was performed using Zen 3.8 (Zeiss) and ImageJ 1.54 d (NIH).

Bacterial 16S rRNA sequencing

Mouse feces were frozen immediately in cryogenic vials (Corning) at −80 °C. 16S rRNA sequencing was performed by DNA Link (Korea). DNA was extracted using the NuceloSpin DNA Stool kit (MACHEREY-NAGEL) according to the manufacturer's protocol. Briefly, 50 mg of mouse feces were added to the NucleoSpin Bead tube and shaken for 10 min. The samples were lysed in 70 °C for 10 min before contents were precipitated, filtered, DNA was bound, and washed. Metagenomic sequencing was performed on an Illumina MiSeq platform (Illumina) targeting 16S rRNA V3 and V4 regions according to manufacturer protocols. Briefly, 16S Amplicon PCR primers used are as following: 5′ TCGTCGGCAGCGTCAGATGTGTATAAGAGACAGCCTACGGGNGGCWGCAG 3′ and 5′ GTCTCGTGGGCTCGGAGATGTGTATAAGAGACAGGACTACHVGGGTATCTAATCC 3′. PCR products were cleaned using AMPure XP beads before Illumina sequencing adapters were added with the Nextera XT Index kit. The library was cleaned again using the AMPure XP beads prior to quantification using automated electrophoresis with TapeStation System (Agilent). The MiSeq v3 reagent kit (Illumina) was used according to the manufacturer's protocol for sequencing. Data were analyzed using MicrobiomeAnalyst2.0[64].

Targeted metabolomics

Targeted metabolomics analyses were conducted at the Clinical Pharmacology Laboratory, Inha University Hospital (Incheon, Korea), using the MxP® Quant 500 kit (Biocrates) in accordance with the manufacturer's protocol. Fresh mouse feces were frozen immediately after collection in cryogenic vials (Corning) at −80 °C. A total of 53 fecal samples were analyzed, with B6 $n = 6$ mice, SPF BTBR $n = 13$ mice, GF BTBR $n = 6$ mice, BTBR-B6 $n = 6$ mice, AVNM $n = 6$ mice, VNM $n = 6$ mice, L. murinus $n = 5$ mice, and IMB015 $n = 5$ mice. Feces were weighed and homogenized for 5 min using stainless steel beads in 1:10 (grams feces: ml buffer) of ethanol/phosphate (85:15, v/v) buffer, before centrifugation (10,000 × g, 10 min) and collection of supernatants.

Targeted profiling of small molecules and lipids was carried out using liquid chromatography–tandem mass spectrometry (LC-MS/MS) and flow injection analysis–tandem mass spectrometry (FIA-MS/MS), respectively. Analysis was performed on an ACQUITY UPLC system (Waters) equipped with a BEH C18 column (1.7 µm, 2.1 × 50 mm), coupled to a Triple Quad 5500+ mass spectrometer (AB Sciex). The system operated with Turbo V electrospray ionization (ESI) in both positive and negative ion modes depending on the analyte class. Ion source parameters included a temperature of 550 °C, spray voltages of +5500 V (positive mode) and −4500 V (negative mode), and a curtain gas pressure of 35 psi. Data acquisition was performed in multiple reaction monitoring mode using predefined transitions provided by the MxP® Quant 500 kit.

LC analysis was conducted using a binary solvent system consisting of 0.2% formic acid in water and acetonitrile, with a 5.8-min gradient as specified by the manufacturer's protocol and previous reports[65]. FIA analysis was performed using a 3-min injection method with the FIA solvent supplied in the kit. Detailed UHPLC and FIA gradient programs are available in the manufacturer's documentation and prior publication[65].

Sample preparation was performed using the Biocrates MxP® Quant 500 kit, which includes isotope-labeled internal standards covering all targeted metabolites. According to the manufacturer's instructions, 10 µL of each sample supernatant was loaded into the 96-well plate. The plates were dried under a gentle nitrogen stream, then derivatized with 5% phenyl isothiocyanate for 1 h. Samples were extracted using 5 mM ammonium acetate in methanol, and the resulting extracts were eluted. For LC analysis, 150 µL of extract was mixed with 150 µL of water, and for FIA analysis, 10 µL of extract was mixed with 490 µL of FIA solvent.

Seven calibration standards containing amino acids and biogenic amines were used to generate standard curves. Quality control (QC) samples at low, medium (QC2), and high concentrations were included and used to assess the intra-assay accuracy of the kit. QC2 was analyzed in triplicate, and the median of these replicates was used to normalize final metabolite concentrations on the plate, referenced to the target concentrations provided by the manufacturer. Additionally, three pooled QC samples were prepared by combining 10 µL from each fecal sample and used for data quality assessment. For quality filtering, only metabolites with a coefficient of variation (CV) ≤ 15% across the pooled QC replicates were retained for downstream analysis.

Quantification was performed according to the standardized Biocrates protocol, utilizing internal standards and calibration curves. Briefly, peak integration and concentration determination were conducted using Analyst 1.7.3 software (AB Sciex), and the resulting data were uploaded into Biocrates MetIDQ® software for further processing. Within MetIDQ, derivatized metabolites—such as amino acids and biogenic amines—were quantified using a 7-point calibration curve and their respective internal standards. In contrast, other small-molecule metabolites and lipids were quantified semi-quantitatively based on signal intensities relative to class-specific stable isotope-labeled internal standards.

Metabolomic data were analyzed using MetaboAnalyst 6.0[66]. Statistical comparisons were conducted using unpaired two-tailed t-tests, with raw $p < 0.05$ considered statistically significant. Volcano plots were generated in MetaboAnalyst, and visualizations of individual metabolite levels were created using GraphPad Prism 10 (Dotmatics).

Statistics

Statistical analyses were performed using GraphPad Prism 10 (Domatics). Data are represented as Mean ± SEM. Two-tailed unpaired Student's or Welch's T-test and one-way or two-way ANOVA were used to calculate statistical significance with p value equal to or less than 0.05 being considered as significant.

Reporting summary

Further information on research design is available in the Nature Portfolio Reporting Summary linked to this article.

Data availability

The authors declare that all data supporting this study are available within the article, source data, and supplementary information files. The data produced and used to generate the figures in this study are provided as source data in the Source Data file. Gating strategy for flow cytometry is available in the Supplementary Information file. The 16S rRNA sequencing, fecal metabolomic analyses, and metabolic flux prediction data for *L. reuteri* IMB015 are available at: https://doi.org/10.6084/m9.figshare.29109347. Raw 16S rRNA sequence data are deposited in the National Center for Biotechnology Information Sequence Read Archive under accession number PRJNA1268144. Custom coding used for metabolite prediction model is available at https://doi.org/10.5281/zenodo.15478642. Source data are provided with this paper.

Code availability

All software programs utilized for this study are available free or commercially. Free and commercially available software utilized in this study include the following: GraphPad Prism 10 (Domatics), WebIDQ (Biocrates), MicrobiomeAnalyst2.0, MetaboAnalyst6.0, Zen 3.8 (Zeiss), ImageJ 1.54 d (NIH), gapseq (committed version 8536a73), sybil R Package (v. 2.2.0), BLASTn (NIH), FlowJo v10.10 (TreeStar), EthoVision XT15 (Noldus), Excel and Word v1808 (Microsoft), and Illustrator v25.1 (Adobe). Specific programs used are detailed within the "Methods" section. Any additional codes for reproduction of the results were developed in R 4.2.2 and python 3.11. and are available in the GitHub repository (https://github.com/IMB-AI/JohnPark-ASD)[63].

References

1. Park, J. C. & Im, S. H. The gut-immune-brain axis in neurodevelopment and neurological disorders. *Microbiome Res. Rep.* **1**, 23 (2022).
2. Sharon, G. et al. Human gut microbiota from autism spectrum disorder promote behavioral symptoms in mice. *Cell* **177**, 1600 (2019).
3. Lewandowska-Pietruszka, Z., Figlerowicz, M. & Mazur-Melewska, K. Microbiota in autism spectrum disorder: a systematic review. *Int. J. Mol. Sci.* **24**, https://doi.org/10.3390/ijms242316660 (2023).
4. Buffington, S. A. et al. Dissecting the contribution of host genetics and the microbiome in complex behaviors. *Cell* **184**, 1740–1756.e1716 (2021).
5. Sgritta, M. et al. Mechanisms underlying microbial-mediated changes in social behavior in mouse models of autism spectrum disorder. *Neuron* **101**, 246 (2019).
6. Buffington, S. A. et al. Microbial reconstitution reverses maternal diet-induced social and synaptic deficits in offspring. *Cell* **165**, 1762–1775 (2016).

7. Hsiao, E. Y. et al. Microbiota modulate behavioral and physiological abnormalities associated with neurodevelopmental disorders. *Cell* **155**, 1451–1463 (2013).

8. Mazzone, L. et al. Precision microbial intervention improves social behavior but not autism severity: a pilot double-blind randomized placebo-controlled trial. *Cell Host Microbe* **32**, https://doi.org/10.1016/j.chom.2023.11.021 (2024).

9. Li, Y. R., Xie, T., Snieder, H. & Hartman, C. A. Associations between autistic and comorbid somatic problems of gastrointestinal disorders, food allergy, pain, and fatigue in adults. *Autism*. https://doi.org/10.1177/13623613241254619 (2024).

10. Park, J. C. & Im, S. H. Of men in mice: the development and application of a humanized gnotobiotic mouse model for microbiome therapeutics. *Exp. Mol. Med.* **52**, 1383–1396 (2020).

11. Zheng, D. P., Liwinski, T. & Elinav, E. Interaction between microbiota and immunity in health and disease. *Cell Res.* **30**, 492–506 (2020).

12. Lu, J. et al. Microbiota influence the development of the brain and behaviors in C57BL/6J mice. *PLoS ONE* **13**, https://doi.org/10.1371/journal.pone.0201829 (2018).

13. Smolders, J. et al. Tissue-resident memory T cells populate the human brain. *Nat. Commun.* **9**, https://doi.org/10.1038/s41467-018-07053-9 (2018).

14. Ito, M. et al. Brain regulatory T cells suppress astrogliosis and potentiate neurological recovery. *Nature* **565**, 246 (2019).

15. Xie, L., Choudhury, G. R., Winters, A., Yang, S. H. & Jin, K. Cerebral regulatory T cells restrain microglia/macrophage-mediated inflammatory responses via IL-10. *Eur. J. Immunol.* **45**, 180–191 (2015).

16. Kim, S. et al. Maternal gut bacteria promote neurodevelopmental abnormalities in mouse offspring. *Nature* **549**, 528 (2017).

17. Alves de Lima, K. et al. Meningeal gammadelta T cells regulate anxiety-like behavior via IL-17a signaling in neurons. *Nat. Immunol.* **21**, 1421–1429 (2020).

18. Meyza, K. Z. & Blanchard, D. C. The BTBR mouse model of idiopathic autism—current view on mechanisms. *Neurosci. Biobehav R.* **76**, 99–110 (2017).

19. McFarlane, H. G. et al. Autism-like behavioral phenotypes in BTBR T +tf/J mice. *Genes, Brain Behav.* **7**, 152–163 (2007).

20. Golubeva, A. V. et al. Microbiota-related changes in bile acid & tryptophan metabolism are associated with gastrointestinal dysfunction in a mouse model of autism. *Ebiomedicine* **24**, 166–178 (2017).

21. Heo, Y., Zhang, Y. B., Gao, D. H., Miller, V. M. & Lawrence, D. A. Aberrant Immune responses in a mouse with behavioral disorders. *PLoS ONE* **6**, https://doi.org/10.1371/journal.pone.0020912 (2011).

22. Angoa-Perez, M., Kane, M. J., Briggs, D. I., Francescutti, D. M. & Kuhn, D. M. Marble burying and nestlet shredding as tests of repetitive, compulsive-like behaviors in mice. *J. Vis. Exp.* https://doi.org/10.3791/50978 (2013).

23. Bove, M. et al. Amygdalar neurotransmission alterations in the BTBR mice model of idiopathic autism. *Transl. Psychiatry* **14**, https://doi.org/10.1038/s41398-024-02905-z (2024).

24. Arakawa, H. Implication of the social function of excessive self-grooming behavior in BTBR T+ltpr3tf/J mice as an idiopathic model of autism. *Physiol. Behav.* **237**, https://doi.org/10.1016/j.physbeh.2021.113432 (2021).

25. Siniscalco, D., Schultz, S., Brigida, A. L. & Antonucci, N. Inflammation and neuro-immune dysregulations in autism spectrum disorders. *Pharma. Base* **11**, https://doi.org/10.3390/ph11020056 (2018).

26. Byun, S. et al. Gut microbiota defines functional direction of colonic regulatory T cells with unique TCR repertoires. *J. Immunol.* **213**, 886–897 (2024).

27. Pasciuto, E. et al. Microglia require CD4 T cells to complete the fetal-to-adult transition. *Cell* **182**, 625 (2020).

28. Liston, A., Dooley, J. & Yshii, L. Brain-resident regulatory T cells and their role in health and disease. *Immunol. Lett.* **248**, 26–30 (2022).

29. Ziv, Y. et al. Immune cells contribute to the maintenance of neurogenesis and spatial learning abilities in adulthood. *Nat. Neurosci.* **9**, 268–275 (2006).

30. Wolf, S. A. et al. CD4-Positive T lymphocytes provide a neuroimmunological link in the control of adult hippocampal neurogenesis. *J. Immunol.* **182**, 3979–3984 (2009).

31. Rattazzi, L. et al. CD4 but not CD8 T cells revert the impaired emotional behavior of immunocompromised mice. *Transl. Psychiatry* **3**, https://doi.org/10.1038/tp.2013.54 (2013).

32. Coretti, L. et al. Gut microbiota features in young children with autism spectrum disorders. *Front. Microbiol.* **9**, https://doi.org/10.3389/fmicb.2018.03146 (2018).

33. De Angelis, M. et al. Fecal microbiota and metabolome of children with autism and pervasive developmental disorder not otherwise specified. *PLoS ONE* **8**, e76993 (2013).

34. Uzunova, G., Pallanti, S. & Hollander, E. Excitatory/inhibitory imbalance in autism spectrum disorders: implications for interventions and therapeutics. *World J. Biol. Psychiatry* **17**, 174–186 (2016).

35. Brown, A., Crowe, L., Andresen, B. S., Anderson, V. & Boneh, A. Neurodevelopmental profiles of children with very long chain acyl-CoA dehydrogenase deficiency diagnosed by newborn screening. *Mol. Genet Metab.* **113**, 278–282 (2014).

36. Wajner, M., Kölker, S., Souza, D. O., Hoffmann, G. F. & De Mello, C. F. Modulation of glutamatergic and GABAergic neurotransmission in glutaryl-CoA dehydrogenase deficiency. *J. Inherit. Metab. Dis.* **27**, 825–828 (2004).

37. Rollan, G., Manca de Nadra, M. C., Pesce de Ruiz Holgado, A. & Oliver, G. Aspartate aminotransferase of Lactobacillus murinus. *Folia Microbiol.* **33**, 344–348 (1988).

38. Zimmermann, J., Kaleta, C. & Waschina, S. gapseq: informed prediction of bacterial metabolic pathways and reconstruction of accurate metabolic models. *Genome Biol.* **22**, https://doi.org/10.1186/s13059-021-02295-1 (2021).

39. Strati, F. et al. New evidences on the altered gut microbiota in autism spectrum disorders. *Microbiome* **5**, https://doi.org/10.1186/s40168-017-0242-1 (2017).

40. Fattorusso, A., Di Genova, L., Dell'Isola, G. B., Mencaroni, E. & Esposito, S. Autism spectrum disorders and the gut microbiota. *Nutrients* **11**, https://doi.org/10.3390/nu11030521 (2019).

41. Sharma, G. et al. A dietary commensal microbe enhances antitumor immunity by activating tumor macrophages to sequester iron. *Nat. Immunol.* **25**, https://doi.org/10.1038/s41590-024-01816-x (2024).

42. Takano, T., Endo, R., Wang, Y. M., Nakajima-Adachi, H. & Hachimura, S. OLL2712 induces IL-10 production by intestinal dendritic cells. *Biosci. Microbiota Food Health* **39**, 39–44 (2020).

43. Nisar, S. et al. Genetics of glutamate and its receptors in autism spectrum disorder. *Mol. Psychiatr.* **27**, 2380–2392 (2022).

44. Hassan, T. H. et al. Blood and brain glutamate levels in children with autistic disorder. *Res. Autism Spectr. Disord.* **7**, 541–548 (2013).

45. Zheng, Z., Zhu, T. T., Qu, Y. & Mu, D. Z. Blood glutamate levels in autism spectrum disorder: a systematic review and meta-analysis. *PLoS ONE* **11**, https://doi.org/10.1371/journal.pone.0158688 (2016).

46. Gevi, F., Belardo, A. & Zolla, L. A metabolomics approach to investigate urine levels of neurotransmitters and related metabolites in autistic children. *Biochim. Biophys. Acta Mol. Basis Dis.* **1866**, https://doi.org/10.1016/j.bbadis.2020.165859 (2020).

47. Ma, B. et al. Altered gut microbiota in chinese children with autism spectrum disorders. *Front. Cell. Infect. Microbiol.* **9**, 40 (2019).

48. Wang, L. et al. Low relative abundances of the mucolytic bacterium Akkermansia muciniphila and Bifidobacterium spp. in feces of children with autism. *Appl. Environ. Microbiol.* **77**, 6718–6721 (2011).

49. Wang, C. et al. A synbiotic formulation of Lactobacillus reuteri and inulin alleviates ASD-like behaviors in a mouse model: the mediating role of the gut-brain axis. *Food Funct.* **15**, 387–400 (2024).

50. Osman, A. et al. Acetate supplementation rescues social deficits and alters transcriptional regulation in prefrontal cortex of Shank3 deficient mice. *Brain, Behav., Immun.* **114**, 311–324 (2023).

51. Pangrazzi, L. et al. The interplay between oxidative stress and inflammation supports autistic-related behaviors in Cntnap2 knockout mice. *Brain, Behav., Immun.* **127**, 57–71 (2025).

52. Cerilli, E. et al. Immune system dysfunction and inflammation in aging Shank3b mutant mice, a model of autism spectrum disorder. *Front. Immunol.* **15**, https://doi.org/10.3389/fimmu.2024.1447385 (2024).

53. Tzanoulinou, S. et al. Inhibition of Trpv4 rescues circuit and social deficits unmasked by acute inflammatory response in a Shank3 mouse model of Autism. *Mol. Psychiatry* **27**, 2080–2094 (2022).

54. Vazana, U. et al. Glutamate-mediated blood-brain barrier opening: implications for neuroprotection and drug delivery. *J. Neurosci.* **36**, 7727–7739 (2016).

55. Lee, H., Chang, M.-J. & Kim, S.-H. Effects of poly-γ-glutamic acid on serum and brain concentrations of glutamate and GABA in diet-induced obese rats. *Nutr. Res. Pract.* **4**, https://doi.org/10.4162/nrp.2010.4.1.23 (2010).

56. Fontaine, C. A. et al. How free of germs is germ-free? Detection of bacterial contamination in a germ free mouse unit. *Gut Microbes* **6**, 225–233 (2015).

57. Wu, W. L. et al. Microbiota regulate social behaviour via stress response neurons in the brain. *Nature* **595**, 409 (2021).

58. Yang, M., Silverman, J. L. & Crawley, J. N. Automated three-chambered social approach task for mice. *Curr. Protoc.* **8.26.1**–**8.26.16**, https://doi.org/10.1002/0471142301.ns0826s56 (2011).

59. Seibenhener, M. L. & Wooten, M. C. Use of the open field maze to measure locomotor and anxiety-like behavior in mice. *J. Vis. Exp.* https://doi.org/10.3791/52434 (2015).

60. Thomas, A. et al. Marble burying reflects a repetitive and perseverative behavior more than novelty-induced anxiety. *Psychopharmacology* **204**, 361–373 (2009).

61. Lee, C. et al. Structural specificities of cell surface beta-glucan polysaccharides determine commensal yeast mediated immunomodulatory activities. *Nat. Commun.* **12**, https://doi.org/10.1038/s41467-021-23929-9 (2021).

62. Dubernet, S., Desmasures, N. & Guéguen, M. A PCR-based method for identification of lactobacilli at the genus level. *FEMS Microbiol. Lett.* **214**, 271–275 (2002).

63. Lee, J. Gut microbiota and brain-resident CD4+ T cells shape behavioral outcomes in autism spectrum disorder. *Zenodo* https://doi.org/10.5281/zenodo.15478642 (2025).

64. Lu, Y. et al. MicrobiomeAnalyst 2.0: comprehensive statistical, functional and integrative analysis of microbiome data. *Nucleic Acids Res* **51**, W310–W318 (2023).

65. Hampel, D., Shahab-Ferdows, S., Kac, G. & Allen, L. H. Evaluating metabolic profiling of human milk using biocrates MxP® QUANT 500 assay. *Metabolites* **15**, https://doi.org/10.3390/metabo15010014 (2025).

66. Pang, Z. et al. MetaboAnalyst 6.0: towards a unified platform for metabolomics data processing, analysis and interpretation. *Nucleic Acids Res.* **52**, W398–W406 (2024).

Acknowledgements

Author contributions

J.C.P., C.H.L., and S.-H.I. designed the project, from its conceptual ideas to the overall outline. J.C.P. designed the experiments, which were performed by J.C.P., C.H.L., and H.P. M.A.S. performed the immuno-fluorescent imaging experiments. J.L. performed the in-silico studies regarding *L. reuteri* IMB015. S.L. provided the *L. reuteri* IMB015 cultures. S.Y.C. organized the 16S rRNA data, which was then analyzed by J.C.P. S.B., H.K., H.L., S.W.K., J.N., and G.P. assisted in performing in vivo immune analyses from mice. J.C.P. wrote the final paper, which was supervised and co-edited by S.-H.I. and T.-K.K.

Competing interests

Additional information